Switching Notes
Note 6
June 1969

Laser Initiated Conduction of an Overvolted Liquid Dielectric

Lt Gilbert L. Zigler
Air Force Institute of Technology
and
Air Force Weapons Laboratory

Abstract

A focused, Q-spoiled laser, aligned along the inter-electrode axis of a pulse charged switch assembly, was used to initiate the conduction of an overvolted transformer oil gap. Laser power varied between 5 and 200 Mw and the voltage pulse exhibited a risetime of 500 nsec to a voltage of 700 kv. A parametric study of the factors affecting the delay between the laser pulse arrival at the gap and conduction of the gap was accomplished, in which the effect of the laser focal point location and power, polarity and voltage on the gap at laser arrival, was determined. Delay times as short as 12 nsec were recorded with jitter, a measure of reproducibility, estimated in the low nanosecond region. Good agreement was found between the observed results and the results predicted from the streamer theory of breakdown.

Contents

Contents (Contd)

List of Figures

List of Figures (Contd)

LASER INITIATED CONDUCTION OF AN OVERVOLTED LIQUID DIELECTRIC

I. Introduction

Statement and Importance of Problem

This research effort is an attempt to determine the suitability of using a giant-pulse laser to initiate the conduction of an overvolted liquid dielectric. In particular, this effort involves a parametric study of the factors affecting the delay to breakdown, i.e., the time interval between the arrival of the laser pulse at the gap and the conduction of the gap, in which the effect of the laser focal point location, laser power, polarity and voltage on the gap at laser arrival was evaluated. Jitter, a measure of reproducibility, of the delay to breakdown was also analyzed as well as the final breakdown voltage. Commercial transformer oil was chosen for this investigation because of its great utility as an insulating liquid.

Laser-triggered switching, LTS, the technique of using a focused, giant-pulse laser to initiate the conduction of a dielectric between charged electrodes, was developed at the Air Force Weapons Laboratory in order to meet the stringent requirements set on switches used in nuclear weapons effects simulation systems. These devices consist primarily of an energy storage system, a switching mechanism, and some form of energy transducer which converts the stored energy into the desired radiation output. The successful simulation of nuclear detonation effects can require voltages in the megavolt region, powers in the thousands of gigawatts with risetimes of less than 10 nanoseconds delivered at the transducer. The main problem is then finding a switch

capable of handling currents in the megampere range that present the minimum inductance to minimize the risetime, while still capable of holding off voltages in the megavolt region. Furthermore, since these systems are now requiring very low impedance operation, the reduction of inductance is very critical since risetime is proportional to the inductance and inversely proportional to the impedance.

Liquid dielectrics are of interest due to the inherit high electrical hold off potentials, especially under a fast pulse where they hold off as much as three to four times their DC breakdown value. This characteristic allows a small gap spacing, hence reducing the switch impedance and inductance. Liquid dielectrics are also amenable to recovery which allows for a quick restoration of their electrical insulation characteristics.

Other reasons for using the laser-triggered switching technique are the inherent safety of a triggering mechanism that is electrically isolated from the high voltage source, its capability of initiating multiple switches with a high degree of synchronization by beam splitting techniques, and, finally, its exhibited capability for repetitive triggering at high rates while still retaining nanosecond jitter.

Survey of Previous Papers

The first paper on laser-triggered switching was published by Guenther and Pendleton (Ref. 15). They focused a 0-80 Mw Q-switched ruby laser perpendicular to the axis of minimum separation of a sphere-sphere gap using different gases as dielectrics, and kilovolt DC voltages. Their preliminary study was involved in determining switching characteristics as functions of laser power, dielectrics gas, gas pressure, gap spacing and electric field. The lowest delay to breakdown,

as low as 10 nsec, was achieved in SF_6 at atmospheric pressure when the laser was focused on the high voltage electrode. Similar results were reported by Barbini (Ref. 2).

To extend LTS to the DC megavolt regime, Guenther and Bettis (Ref. 11) used a 100-250 Mw ruby laser to trigger a 50 ohm coaxial capacitor by firing the laser along the inter-electrode axis. Gases were used as dielectrics and delays to breakdown of 2 nsec with jitters of 0.2 nsec were reported.

The use of high vacuum as a dielectric for LTS was studied by Clark, et. al. (Ref. 5) using a 1 Mw Q-switched ruby laser triggering a 300 kv DC gap. Delays to breakdown in low microsecond region were observed.

Repetitive LTS was reported by Guenther and McKnight (Ref. 13) by using a low-energy high brightness YAG laser to switch a gas gap. Repetition rates of 50 pulses per second with jitter less than 1 nsec were reported. Multi-gap switching and multi-channel switching in DC gases were also studied by Guenther, et. al. Four gas gaps were fired at 50 pulses per second within .1 nsec of each other by using a YAG laser (Ref. 12) and the simultaneous laser initiation of two breakdown channels in a single gap reduced the current risetime of the output by a factor of two when compared to a single channel breakdown (Ref. 9).

The use of solid dielectric for LTS was investigated by Strickland (Ref. 21). He employed a 20-90 Mw Q-switched ruby laser focused along the inter-electrode axis with DC voltages of 80 kv, obtaining delays to breakdown as low as 3 nsec in 10 mil Lexan.

One other dielectric has been investigated for use in LTS. Marolda (Ref. 14) used transformer oil in a sphere-sphere gap with

spacing of 0.365 cm and studied two triggering configurations for DC LTS breakdowns. Microsecond delays were observed when the laser was focused perpendicular to the inter-electrode axis whereas delays as low as 30 nsec were observed when the laser was focused along the inter-electrode axis.

Organization of Paper

The body of this paper contains six main chapters. Chapter II will present a brief outline of the available mechanisms for electron production and borrows the two main breakdown mechanisms from gaseous breakdown to form a semi-quantitative expression for the laser initiated breakdown of an overvolted transformer oil. Chapter III explains the equipment used in this experiment, including a discussion of the operation of a Marx pulse generator. Chapter IV explains the experimental arrangement, including a description of the degradation of the equipment. Chapter V defines the parameters to be varied and discusses how these parameters were obtained. The main results are presented at the end of this chapter. The last chapter, Chapter VI, contains a discussion of the data and how it correlates with the semi-qualitative proposed expression developed in Chapter II and an estimation of the errors present in the various measured parameters. Possible solutions to the problems encountered are suggested. This last chapter ends with recommendations for further studies, and the applicability of employing the LTS technique to an overvolted liquid dielectric.

II. Theory

A rigorous theory of the breakdown mechanism of liquid dielectrics under DC or pulsed voltages is as yet not available. The following four sections will attempt to describe the principal phenomena associated with overvolted breakdown of a liquid dielectric when the dielectric breakdown is initiated by a laser.

The first section deals with the mechanisms available to liberate ions and electrons from the surface of the electrodes, followed by a section describing the events that follow the liberation, mainly the mechanisms of ionization and deionization. The third section describes the mechanisms available to explain the conduction and breakdown of the gap. The last section will attempt to place the first three areas together and semi-quantitatively describe the laser initiated breakdown.

The voltage pulse associated with this experiment can be considered a ramp function going from zero to 700 kv in 400 nsec.

Emission of Electrons and Ions from the Electrodes

Two major mechanisms are involved in this experiment. The first type deals with the electron and ion emission before the laser pulse arrives; the latter with the emission at laser arrival.

Before the laser pulse arrives in the switch area, the electrodes are under the influence of a ramp voltage pulse. Under these conditions, the main mechanism of electron emission is due to field effect emission. Ion emission at this state is negligible.

Field Emission

Under the action of an electric field, electrons may be "pulled" out of cold surfaces by the field along (Ref. 6). This effect is

known by several names, mainly as field emission, cold emission or auto-electronic emission. An expression based on the wave mechanics theory has been developed by Fowler and Nordheim for this type of action under an electrostatic field. The Fowler-Nordheim equation for the field emission rate of electron generation is of the form:

$$dn/dt = A\ E^2 \exp(-B/E) \tag{1}$$

where:

A and B are constants

E = electrostatic field

In order to describe a time dependent electric field, assume that the voltage pulse applied to the target electrode is:

$$V = V_o\ t \tag{2}$$

then the electric field associated with this ramp voltage pulse is:

$$E = E_o\ t \tag{3}$$

for the electric field is:

$$E = V/d$$

and

$$E_o = V_o/d$$

where d is the gap spacing.

Hence, the rate of electron generation by field emission becomes:

$$dn/dt = A^*\ t^2 \exp(-B^*/t) \tag{4}$$

where: $A^* = AE_o^2$

and $B^* = B/E_o$

It should be noted that the surface fields may be quite high in value with respect to the average field due to the presence of slight irregularities on the surface of metal. This field enhancement will be markedly noticed in case of this experiment due to the fact that the electrodes were not polished nor replaced throughout the experiment. Figure 16, found under the section dealing with equipment degradation, depicts the target electrode condition after approximately sixty shots.

Electron and Ion Emission by Laser Pulse

Once the laser pulse arrives at the target electrode the entire electron emission picture is greatly changed. The interaction of the laser pulse radiation with a solid surface may be described phenomenologically as the electronic absorption of the optical radiation by the cold surface within a few optical mean free paths of the surface during the first few nanoseconds of the energy deposition cycle of the laser pulse, with the consequent vaporization of the material. Further heating of the cool vapor may then occur at somewhat later times during the laser pulse due to molecular absorption, with the eventual ionization and reradiation from the plasma. Figure 1 shows the interaction of the laser with the target electrode without any voltage applied to the target electrode. Note the plasma formation due to the heating of the blow-off material.

Due to the complexity of the interacting individual phenomena of electron and ion formation caused by the laser, it is beyond the scope of this study to relate each individual mechanism of ion and electron

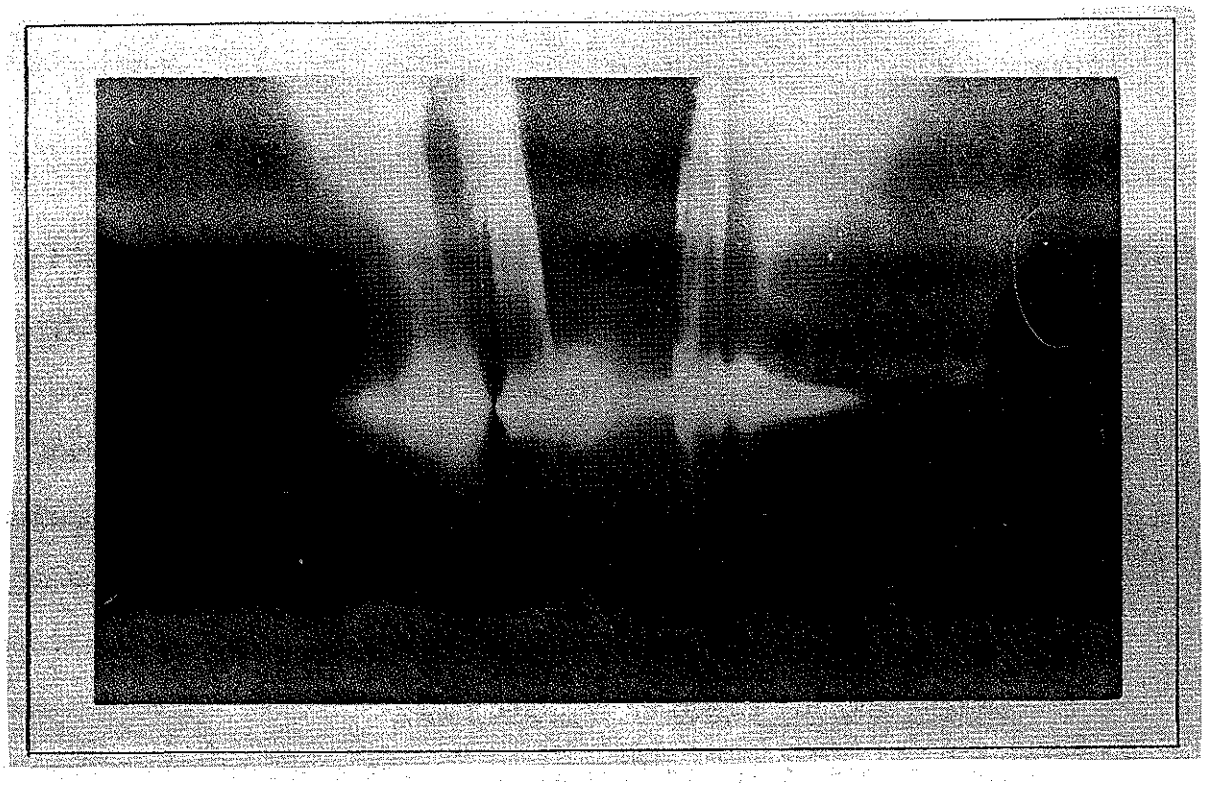

Fig. 1 Laser Pulse Interaction with the Target Electrode

(Target electrode is on the left and the laser pulse is travelling from right to left.)

production. Instead, an overall electron generation equation developed by Raizer will be employed (Ref. 17).

The equation described by Raizer for the rate of electron generation in plasma by a laser is:

$$dn/dt = N_o \, \theta \exp(\theta t) \tag{5}$$

where:

N_o = number of electrons present at laser arrival.

θ = number of electrons produced per second.

t = time in seconds

This expression will hold true for only the middle portion of the laser pulse. The limits to be set on the middle portion of the laser pulse are arbitrary, for equation (5) is not valid for the fast expanding plasma encountered during the latter portion of the laser pulse interaction. The plasma of interest is formed during the first few nanoseconds of the laser pulse.

The number of electrons present at laser arrival will be determined by the combination of the electrons produced during the field emission and the assumed constant number of electrons generated by the initial few nanoseconds of the laser. During the early stages of the voltage pulse on the target electrode, the field emission electrons can be neglected, a condition which does not hold true at voltages near self-breakdown of the dielectric.

Ionization and Deionization of the Dielectric Media

Once the electrons and ions have been injected into the dielectric medium they will start drifting under the influence of the electric field and cause ionization of the dielectric medium or be lost due to recombination.

In order to separate the mechanisms of electrons production and recombination, the following assumptions will be made:

1. There exists a large number of electrons and ions in the dielectric with a wide energy spread caused by the previously mentioned mechanisms.

2. The laser has little effect on the dielectric due to photoionization, for measurements made of the absorption of the dielectric used in this experiment showed an almost 100% transmission of the 6943A°

radiation of the laser.

3. The effect of the magnetic field associated with the pulsed electric field is insignificant. This is due to the fact that the ratio of the electric field to the magnetic field can be related as:

$$R = E/(Bv/c) \tag{6}$$

Where:

E = electric field

B = magnetic field

v = velocity of the particle

c = velocity of light

The maximum particle velocities are small compared to that of the speed of light, causing the ratio to heavily favor the electric field force.

The main mechanisms of ionization and deionization are ionization by electron collision, radiation ionization, and recombination.

Ionization by Electron Collisions

The energy necessary to ionize a molecule of the dielectric media may be given to the molecule by means of an electron impact. The effectiveness of the electron to cause ionization depends on its energy. It is customary to determine a quantity S, a probability of ionization by an electron, basically related to the number of ion pairs produced by the electron travelling one centimeter in the dielectric. S will be small for electron energies below the ionization potential of the dielectric and will again decrease when the electron is too energetic.

Moderate speed electrons having energy less than the ionization potential may excite an atom and this excited atom may be struck by another slow moving electron, thereby gaining enough energy to complete the ionization. Very fast electrons are also poor ionizers compared to those of optimum energy for they can pass through the atom's sphere of influence without removing an electron.

If the colliding electron has more energy than the minimum necessary to ionize the atom, the excess may be transferred to the ejected electron, be retained by the ionizing electron or may be retained by the single ionized atom and cause further excitation or ionization. Any combination of these events can occur. In considering the processes involved in the electron collision one must remember that the laws of conservation of energy and momentum must hold for the immediate products of the collision. In polyatomic molecules the internal energy of the resulting positive ion may be greater than the energy of its disassociated fragments so that the disassociation may result in secondary products of ionization.

Positive ions are effective ionizing agents if their energies are very large. Ions apparently become effective ionizers when their velocities are as great as those of electrons which have attained energies comparable to the ionization potential of the dielectric. The effect of positive ion can be neglected for they are assumed not to have attained enough energies to become effective for ionization.

Radiation Ionization

Radiation ionization or photoionization is the term applied to the capability of a photon to ionize a substance. The heated plasma formed by the laser is a source of considerable range of wavelengths.

The photons emitted by recombination of electrons in the trailing edge of avalanches (as will be further explained) is also an intense source of ionizing radiation. It should be remembered that the laser at 6943A° does not have sufficient energy to cause ionization of the molecules.

Photons having energies less than the minimum ionization potential of the dielectric will cause no ionization while those of higher energies than the ionization potential will eject electrons of high energies. This secondary electron could then produce more ionization by electron collisions.

Recombination

The main mechanism of deionization will be considered the recombination process. Attachment mechanisms have a very slight probability of occurrence for they require a third body to accept the excess energy of the attaching particles (Ref. 6).

Consider a volume of gas in which ions of both signs are uniformly distributed and ionizing effects have been removed. It will be assumed that in this region there exists a high density of ions. The rate of disappearance of ions of either sign should be proportional to the product of the density of the two kinds.

Let:

N_1 = density of negative ions

N_2 = density of positive ions

γ = recombination coefficient

then:
$$dN_1/dt = dN_2/dt = N_1 N_2 \gamma \qquad (7)$$

If the positive and negative ion concentrations are equal and of density N, the equation (7) becomes:

$$dN/dt = \gamma N^2 \tag{8}$$

Using the mechanisms presented above, an attempt will now be made to describe a suitable breakdown mechanism.

Breakdown Mechanisms

Due to the complex nature of the processes in overvolted liquid dielectrics, no satisfactory breakdown expressions have yet been developed. This study will adopt the two accepted breakdown mechanisms available from gas breakdown and try to relate them to liquid dielectrics. These mechanisms are the Townsend avalanche and streamer mechanisms.

Townsend Avalanche Breakdown

The Townsend avalanche breakdown mechanism is based solely on field intensified ionization by charged particle collisions. Basically, one assumes that there exists a number of charged particles, available at the electrode, which start drifting under the influence of the electric field. Since the positive ions only produce sufficient ionization if greatly accelerated, they will be neglected. If one then assumes that the electron can produce α ionizing collisions per centimeter of travel, the total number of electrons generated after a distance x can be computed from:

$$N = N_o \exp(\alpha x) \quad \text{(Ref. 18)} \tag{9}$$

where: N_o = initial number of electrons

If one assumes that:

$$\beta = \alpha x/t$$

where: t = average time taken by the electron to cover a distance x

one obtains an expression for the total number of electrons after a time t.

$$N = N_o \exp (\beta t) \tag{10}$$

Differentiating Eq (10) with respect to time, one obtains an expression for the rate of charge carrier production due to the Townsend avalanche mechanism:

$$dN/dt = N_o \beta \exp (\beta t) \tag{11}$$

The exponential growth of the number of electrons produced by the Townsend avalanche mechanism can be physically interpreted as a conical-shaped growth of ionization. The avalanche process continues until the gap is bridged with an ionized path along which conduction can take place.

This rather simple theory can account to some extent for the self-breakdown of the pulsed dielectric. Another mechanism, nevertheless, has to be proposed in order to explain certain characteristics of the laser induced breakdown. This other process is the streamer mechanism.

Streamer Mechanism

The streamer breakdown mechanism was first proposed in 1936 by Raether and Fleger (Ref. 18). This theory is an avalanche related

mechanism and relies on photoionization of the dielectric produced during the avalanche.

Assume that the avalanche crosses to mid-gap or near the anode. At a certain point in the growth of this avalanche, the positive ion density in the trailing portion of the avalanche (anode end) becomes sufficient to produce local fields which distort and augment the applied field. If these local fields are high enough, the electrons emitted from the head of the avalanche will tend to recombine with the positive ions in the avalanche and emit high energy recombination photons isotropically, which causes photoelectric ionization. In the intense field regions ahead of and behind the avalanche head, the photoelectric ions produce new avalanches and rapidly spread the discharge towards both electrodes.

The required field distortion caused by the positive charge density trailing one avalanche may not be sufficient for streamer formation. In this case several avalanches are needed so that the space charge formed by each successive avalanche would then add to the space formed by the preceding avalanche until the cumulative space charge field distortion is sufficient to produce streamers.

In an avalanche or streamer directed towards the anode, the electrons ahead of the propagating discharge are swept to the anode away from the growth of ionization. However, if one has the discharge initiated at the anode, the extremely high-positive charge at the head of the propagating arc column accelerates electrons towards itself with such force that copious numbers of ionizing collisions can take place, resulting in emission of high-energy photons, which now travelling at the speed of light in the dielectric, can produce ionization of the

dielectric media and, therefore, quickly bridge the gap.

Two basic important differences between the two breakdown mechanisms should be observed. First, the streamer mechanism is faster due to its reliance on photons rather than electrons for the breakdown propagation. Second, the streamer mechanism can propagate from the anode to the cathode whereas the avalanche can not.

Laser Initiated Conduction

The first three sections of this chapter have dealt with the available mechanisms of producing electrons and ions at the electrodes and the dielectric. These sections have supplied the basic tools necessary to attempt to describe the laser induced breakdown.

Two important processes are now assumed evident:

1. Conduction of the gap will occur through an avalanche streamer process.

2. The streamer propagation is so rapid that the delay between the initial production of charge carriers and the breakdown is essentially the time it takes the avalanche to reach the critical charge carrier concentration to form streamers.

The basic approach will be to form an equation relating the net rate of electron production by the previous mechanisms. This net rate of electron production can be integrated from 0 to the time of breakdown, giving the critical charge carrier concentration needed for conduction. The net rate of electron generation will then be the sum of the electrons produced by field emission, laser and Townsend avalanche minus the electrons lost due to recombination:

$$\begin{bmatrix}\text{net rate of}\\ \text{electron}\\ \text{production}\end{bmatrix} = \begin{bmatrix}\text{rate of electron}\\ \text{production by}\\ \text{field emission}\end{bmatrix} +$$

$$\begin{bmatrix}\text{rate of electron}\\ \text{production by}\\ \text{laser}\end{bmatrix} + \begin{bmatrix}\text{rate of electron}\\ \text{production by}\\ \text{Townsend avalanche}\end{bmatrix} -$$

$$- \begin{bmatrix}\text{rate of electron}\\ \text{recombination}\end{bmatrix}$$

Using the previously described equations, mainly Eq (4), (5), (11) and (8), one can write the above expression as:

$$dN/dt = A^*t \exp(-B^*/t) + N_o\, \theta \exp(\theta\, t) + N_o'\, \beta \exp(\beta\, t) - (N_o'')^2\, \gamma \qquad (12)$$

Since these terms apply only to distinct sections of the total electron generation time, a discussion of the time elements and significance of the associated constants follows.

The rate of electron generation by field emission has time limits from t=0 to t=breakdown. The contribution of this term can be considered small as compared to the total number of electrons generated by the other two mechanisms.

The rate of electron production by laser term has limits from t = (laser arrival + dt) to t = end of laser pulse. The constant N_o, the number of electrons present at laser arrival, will be the number of electrons generated by plasma boil-off from the target electrode during the first portion of the laser interaction.

The rate of electron generation by Townsend avalanche term has

limits from t=0 to t=breakdown time or until streamers take over. The constant N_o' will be time dependent and will basically be the number of electrons generated by the preceding terms of electron generation.

The rate of recombination term is present throughout the entire electron generation time, mainly from t=0 to t=breakdown time. The constant N_o'' will be time dependent and will essentially be the number of electrons generated by the three preceding electron generation terms.

The net rate of electron generation equation will not be integrated but kept as is so as to maintain the different generation terms independent.

III. Equipment

The laser triggered apparatus used in this experiment consists of four major components: an electronically Q-switched laser, an optical conduit housing a lens system for focusing the laser radiation, a 2 Megavolt Pulser, and the diagnostic equipment. These four major components are depicted in Fig. 2.

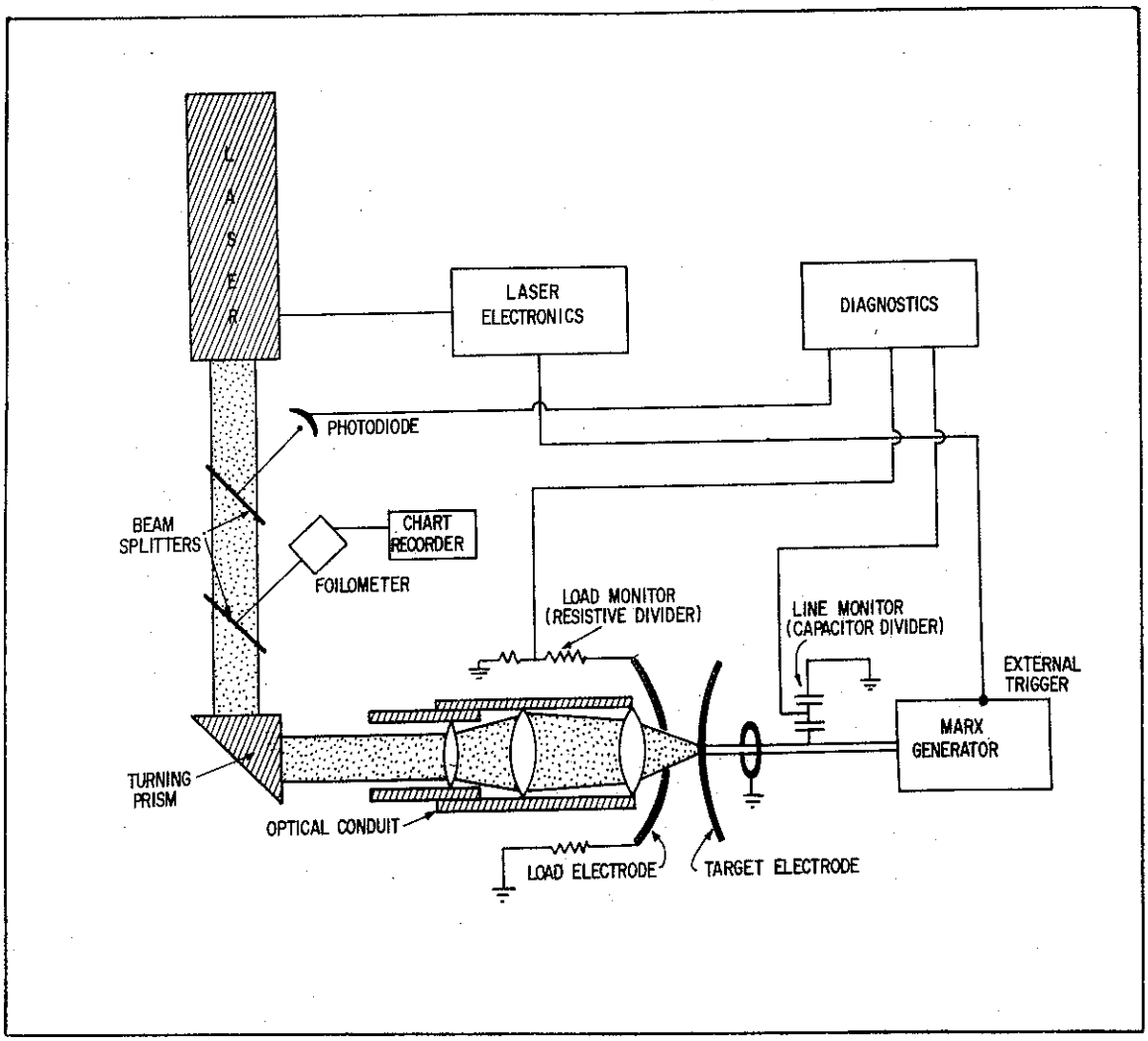

Fig. 2 Major Components of the Laser-Triggered Switching Apparatus

Laser System

The laser system used in this experiment was an oscillator-amplifier

Korad model K-1500 ruby laser. Energy output of the laser system could be continuously varied from 1 to 8 joules with pulse widths (FWHM) from 40 nsec for the lower energy range to 30 nsec for the higher energy range. Peak powers varied from 20 to 220 Mw. Figure 3 depicts the laser system.

This system employs an oscillator rod, 9/16 inches in diameter by 6 inches long oscillator rod, optically pumped by a single helical Xenon flashlamp. This assembly is placed in an optical cavity Q-spoiled by a KD*P Pockels cell. When the Pockels cell is triggered electronically on command, the oscillator cavity is completed by a 100% dielectric reflector at the rear and a 17% reflectivity sapphire flat in the front. The entire oscillator cavity is approximately 24 inches long, from rear reflector to front reflector.

The output of the oscillator is passed through an inverse Galilean telescope which expands the beam to approximately 3/4 inches in diameter. The beam is then apertured by an elliptical ceramic assembly whose function is to prevent blow-off onto the face of the amplifier rod from the aluminum amplifier rod holder.

After the oscillator output is apertured it is allowed to pass onto the amplifier stage placed at the Brewster angle with respect to the oscillator axis. The amplifier stage is comprised of a ruby rod, 3/4 inches in diameter by 9 inches long, optically pumped by a single helical Xenon flash lamp. The output of the laser system is then allowed to pass through a Brillouin reflection rejection system comprised of a Brewster's plate tent horizontally polarized, followed by a quarter wavelength plate cut for the ruby wavelength, 6943A°. The functions of this Brillouin reflection rejection system will be

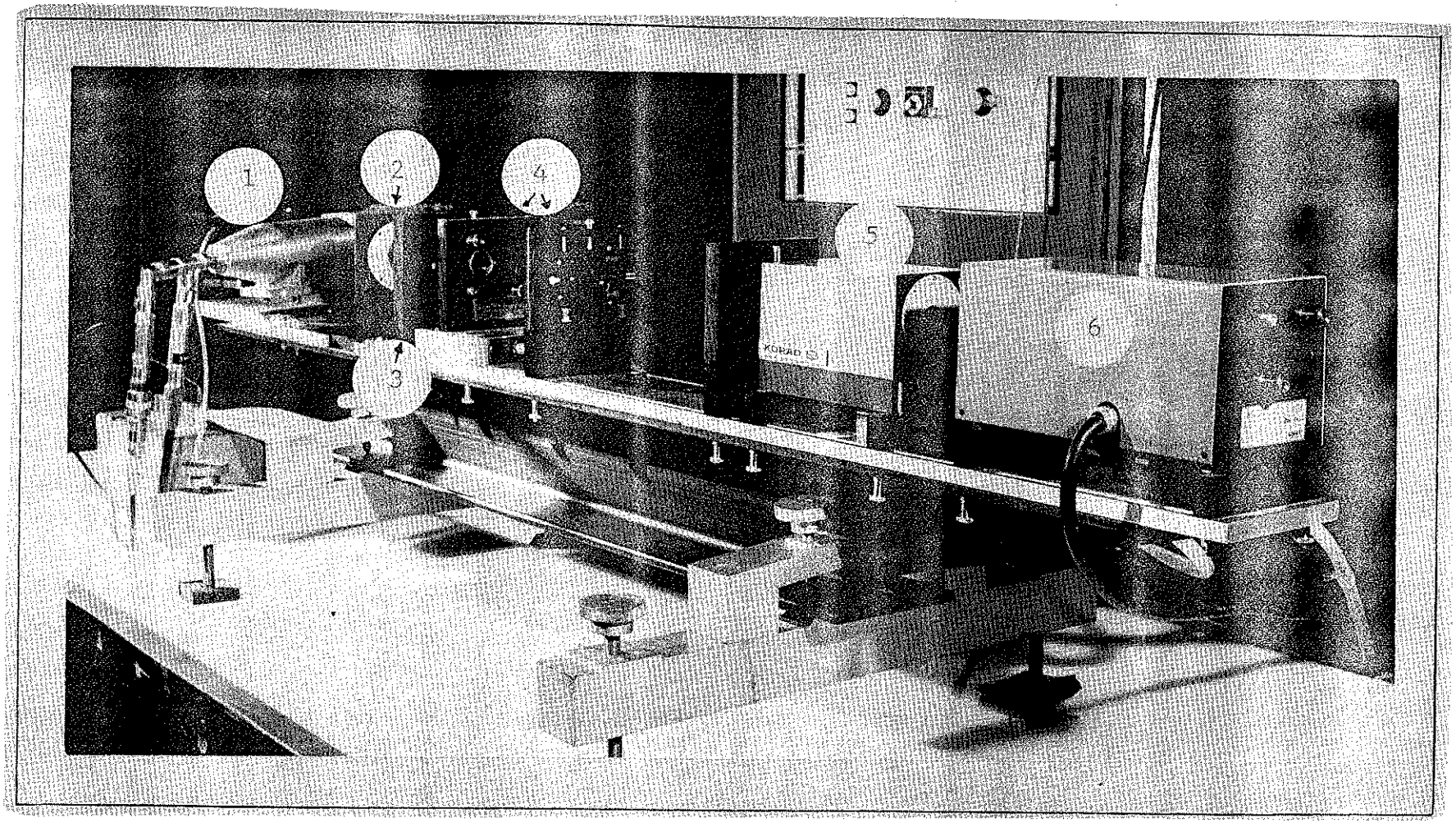

Fig. 3 Laser System

1 - Diagnostics (Laser)
2 - Amplifier
3 - Aperture
4 - Telescope
5 - Oscillator
6 - Pockels Cell

discussed in the section dealing with equipment degradation, page 40.

Laser Electronics

The laser electronics consist of the laser capacitor bank, shutter electronics A, a delay generator and shutter electronics B.

The laser capacitor bank consists of a 60 uf capacitor used on the oscillator flashlamp and four 100 uf capacitors used on the amplifier flashlamp. The amplifier flashlamp capacitors could be inserted in the system in any number.

Shutter electronics A consists mainly of a millisecond delay generator, whereas the delay generator consists of an El Dorado Model 650 nanosecond delay generator. Shutter electronics A is used to set the opening of the Pockels cell at maximum population inversion of the oscillator rod, whereas the delay generator is used to time sequence the laser pulse at different times on the voltage ramp applied to the target electrode.

Shutter electronics B is the originator of a 40 kv pulse used to command the opening of the Pockels cell. This 40 kv pulse was achieved by shorting a coaxial line charged to 20 kv and using voltage doubling of the reflected pulse. The time the Pockels cell was kept opened is determined by doubling the electrical transit time of the charged cable.

Optical System

The optical system consists of a turning prism and an optical conduit. The turning prism is a 45-90-45 degree prism whose perpendicular faces are coated with a hard anti-reflecting coating for 6943A° in order to insure minimum reflectivity of the laser output back into the laser system.

The optical conduit was designed to transport the laser radiation through the load chamber of the 2 Mv pulser and allow it to be focused along a line joining the points of closest approach of the electrodes. The conduit consisted of a plexiglass tube in which three lenses were mounted. This assembly was hermetically sealed in order to insure that none of the SF_6 used to pressurize the load chamber would penetrate the lens system, thereby changing the index of refraction of the media in which the lens were exposed. The entrance end was opened to the atmosphere whereas the exit end was exposed to the dielectric in the switch chamber. This exit end was sealed by the last lens and a high pressure nozzle was provided to circulate the dielectric in the switch chamber over this final lens in order to insure that air bubbles or carbon caused by the laser breakdown of the dielectric would not interfere with the passage of future laser pulses. The three-lens system description and governing equations, together with the theoretical and experimental focus positions plots, can be found in Appendix A.

2 Megavolt Pulser

The pulse generator used in this experiment was a Physics International 2 Mv Pulser. This system has the capability of delivering a 2 megavolt pulse with a rise time of 700 nsec to a 24 inch in diameter semielliptical electrode. Figure 4 is a cross-sectional view of the 2 Mv pulser. In Fig. 5, its exterior is shown.

The 2 Mv pulser consists of five subassemblies: (1) the control console and Marx trigger amplifier, (2) a DC power supply, (3) a 15 stage Marx generator, (4) a 10 ohm coaxial line and (5) the switch and load assembly.

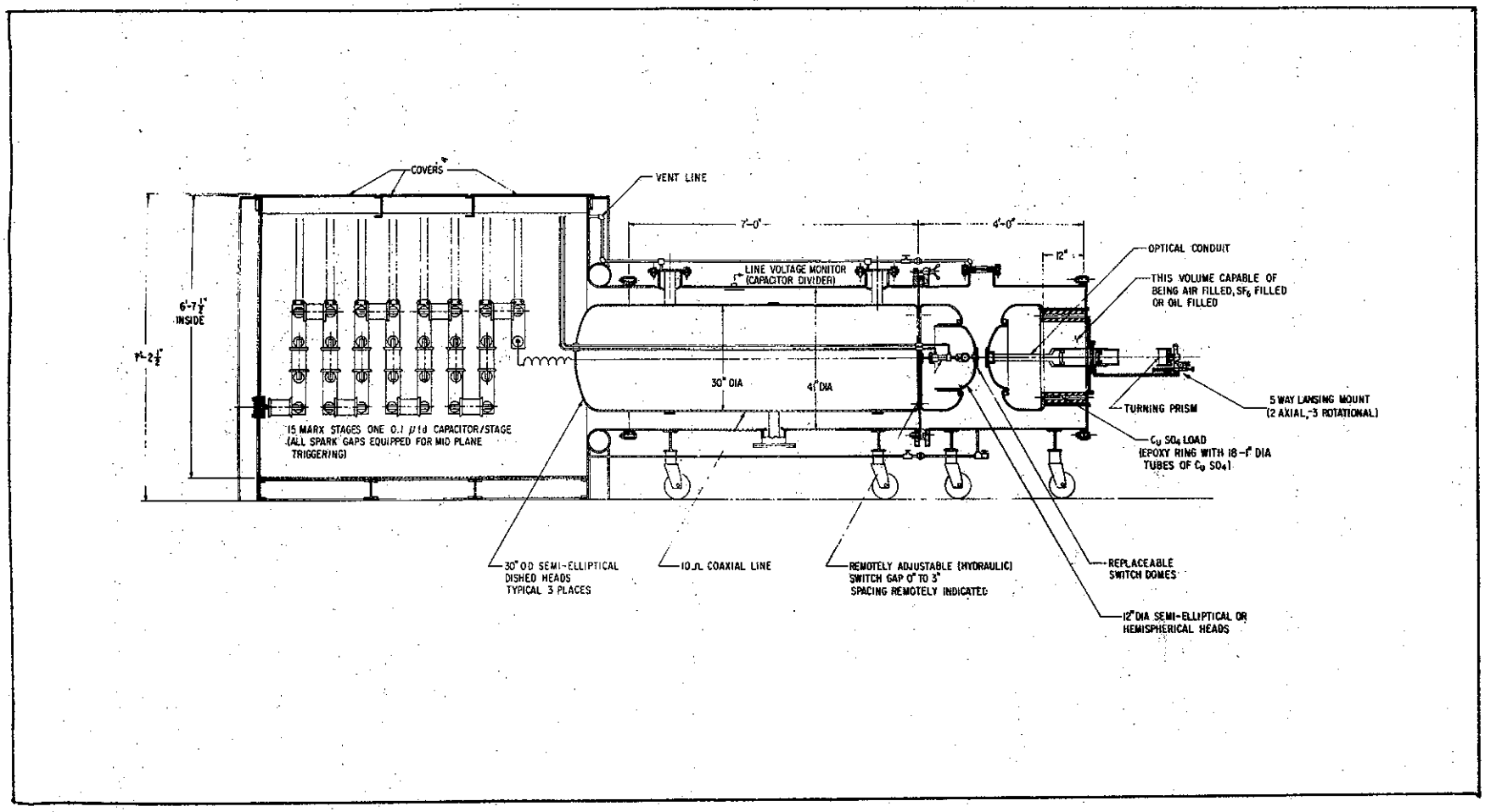

Fig. 4 Cross-sectional View of the 2 Mv Pulser

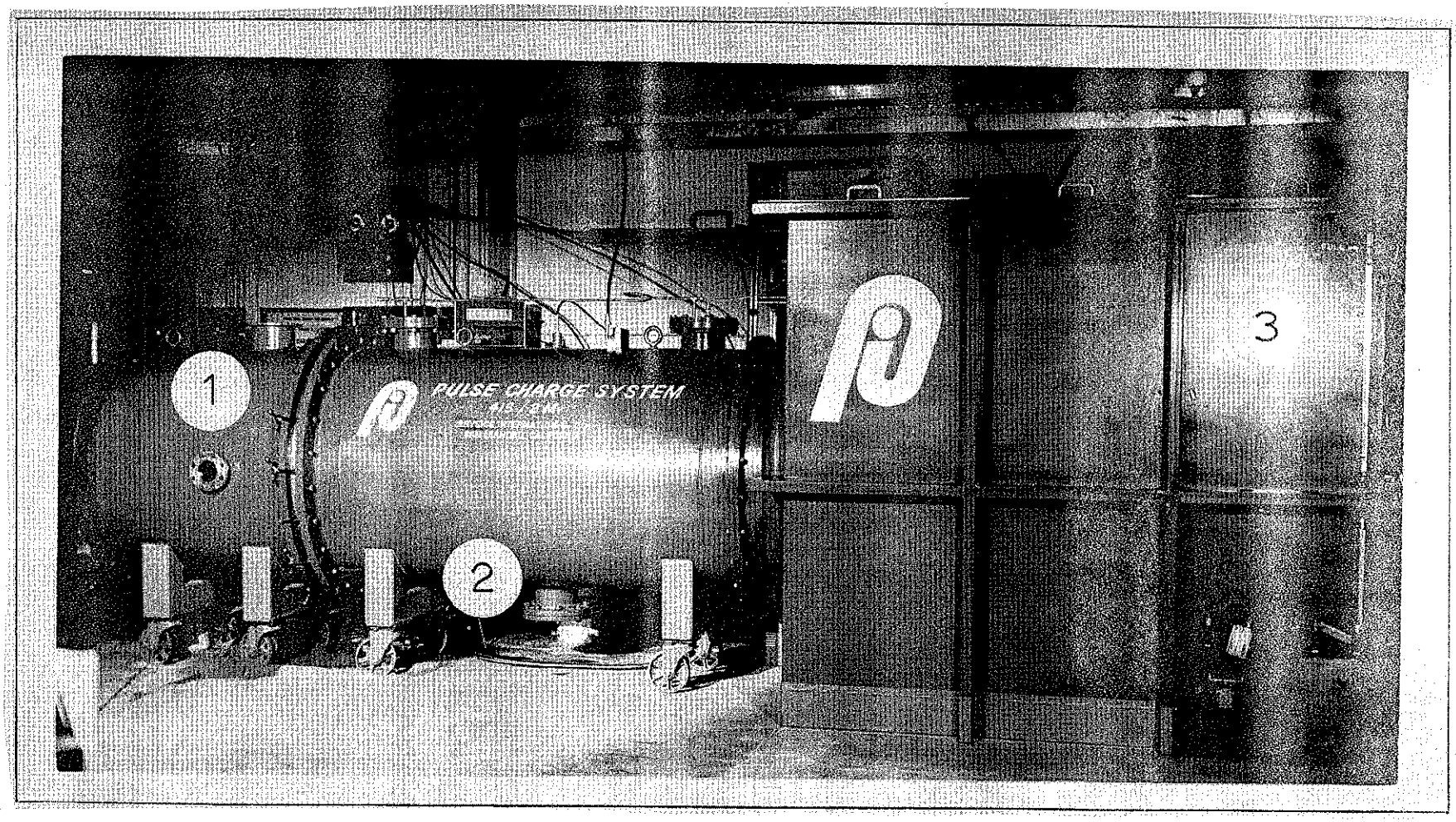

Fig. 5 Exterior View of the 2 Mv Pulser

1 - Switch Chamber 2 - Coaxial Line 3 - Marx Generator

Control Console and Marx Trigger Amplifier

The operation of the 2 Mv pulser is controlled and monitored from this console. To assure the charging voltage of the Marx generator, two meters, each with its own metering string, were used; one to measure the voltage on the DC power supply and one to indicate the voltage to which one of the Marx stages had been charged.

Mounted on the control console is a trigger amplifier that generates the high level signal required to trigger the first spark gap. A portion of the output pulse from the trigger amplifier output was used to synchronize other electrical equipment with the Marx generator operation.

DC Power Supply

The DC power supply charges the Marx generator and is controlled by a variable transformer situated on the control console. The charging voltage can be varied continually from 0 to 100 kv at a maximum charging current of 10 ma. If the charging current exceeds 10 ma, the Marx generator is automatically discharged.

Marx Generator

The Marx generator has 15 stages of 0.1 uf capacitance with a total equivalent series capacitance of 6660 pf and total stray inductance of 10.0 uh, and is capable of storing 4800 joules at an 80 kv charging voltage. Figure 6 is a schematic representation of the Marx generator circuit.

Each of the Marx stages is in fact two capacitors contained in one case and connected in series between the terminals with the mid-point connection of the two capacitors connected to the case. The Marx stages are connected in series through modular mid-plane

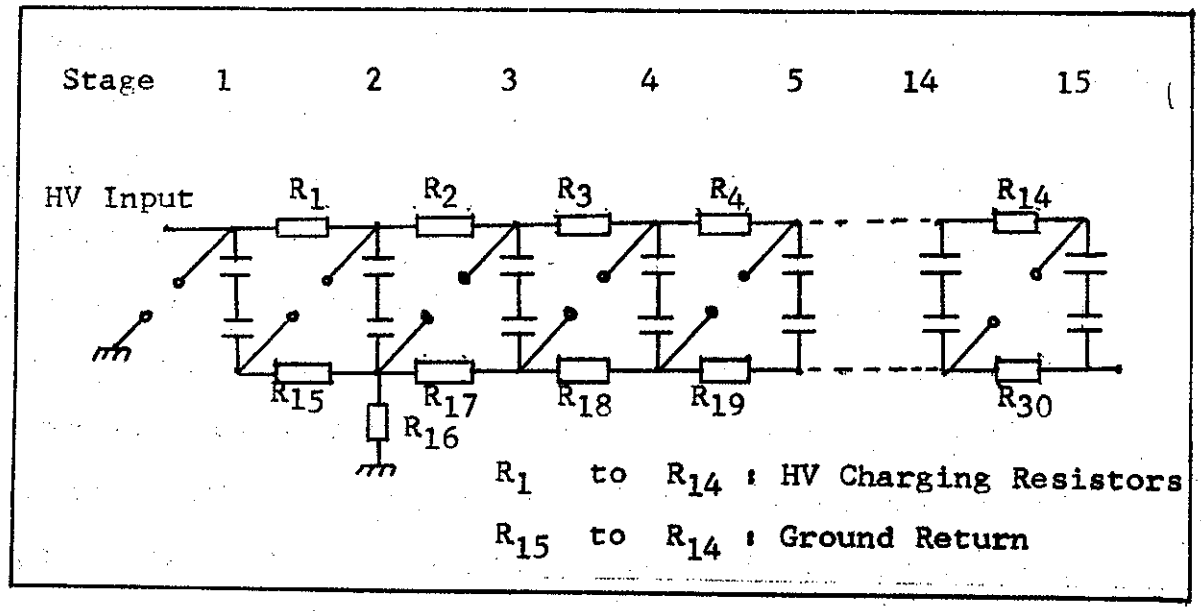

Fig. 6A Equivalent Marx Generator Configuration During Charging

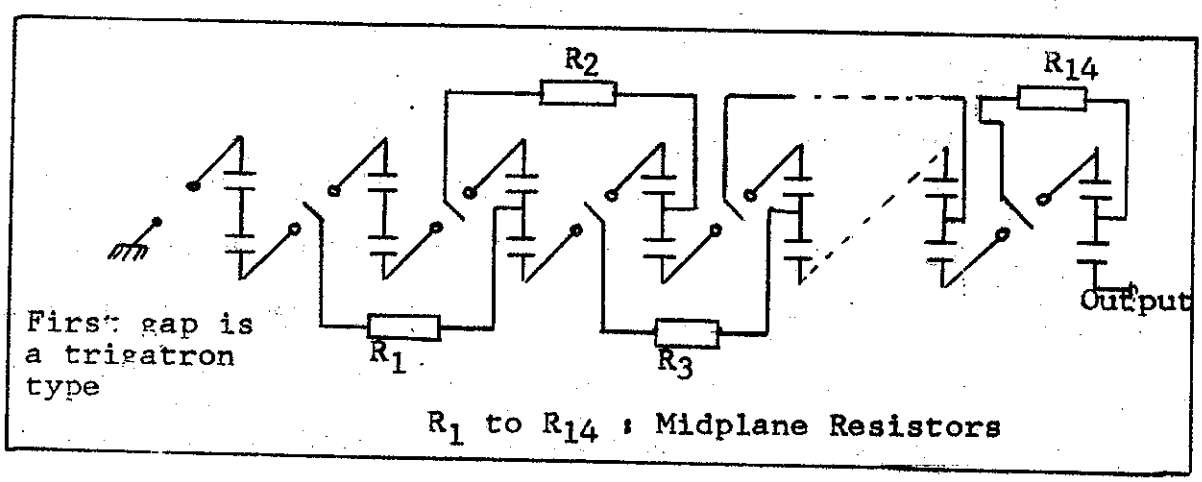

Fig. 6B Equivalent Marx Generator Configuration During Erection

triggered spark gaps pressurized with SF_6 gas. The mid-planes of each gap are resistively tied to the capacitor case two stages ahead. During the charging of the generator the resistance across the mid-plane gap is too large and the generator charges as a sequence of parallel capacitors through the charging resistors. The mid-planes are held at their equipotential, i.e., one half of the charging voltage, during the charging and holding operations. A trigatron gap, using compressed air as dielectric, is connected between the first stage and ground. When the first stage is shorted to ground on command from the Marx trigger amplifier, the mid-planes become unbalanced with respect to the main electrodes and erection of the Marx generator takes place. The use of the mid-plane triggered spark gaps makes it possible to reduce the jitter and erection time of the Marx generator. The output of the Marx generator is used to pulse charge the 10 ohm coaxial line through a large inductor.

10 Ohm Coaxial Line

Connecting the Marx generator and the target electrode is a 10 ohm coaxial line. This line is pulse charged by the Marx generator via a 40 uh choke. The coaxial line measures 8 ft. long, with the inside conductor having a diameter of 36 inches and the outside conductor 48 inches. The total line capacitance is calculated to be 1200 pf, with transformer oil used as the dielectric between the outside and inside conductor. Situated at the middle of the coaxial line is a capacitive voltage divider which monitors the pulse charge and the reflection from the load on the 10 ohm line. The pulse charging equations can be found in Appendix B, together with the experimentally determined voltage waveforms.

Switch Chamber and Load Assembly

A separate chamber contains the electrodes forming the switch and the load assembly. A cross-sectional view of the switch and load assembly is shown in Fig. 7.

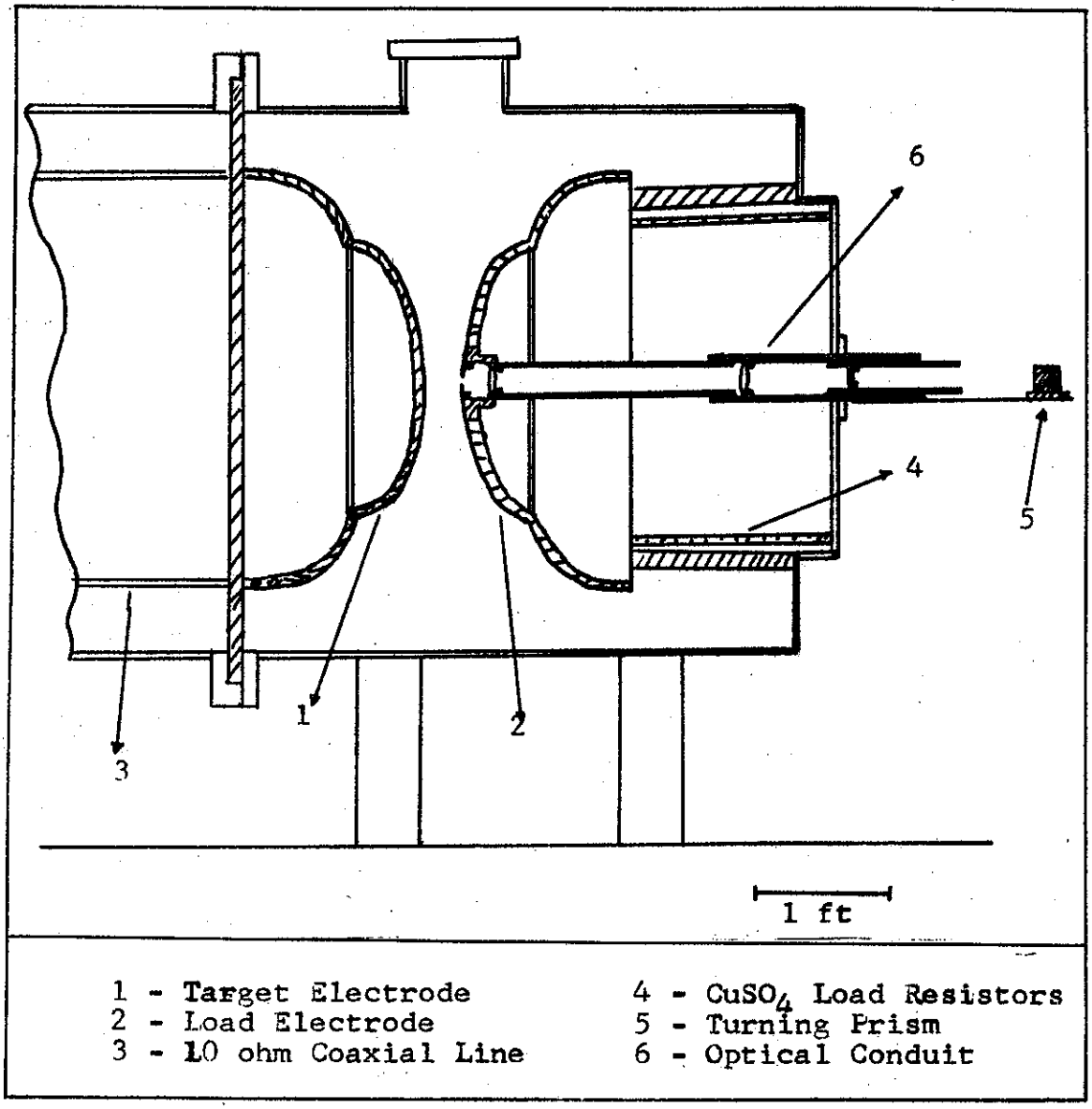

Fig. 7 Cross-sectional View of the Switch Chamber and Load Assembly

Connected directly to the 10 ohm line is the target electrode. The load electrode across the gap is supported by an insulating ring

of epoxy. The target electrode can be externally adjusted by a hydraulic system to vary the gap spacing. Thirty-two 320 ohm copper sulfate resistors form a parallel bridge across the epoxy vessel grounding the load electrode. The total impedance of the load is 10 ohms, which matches the impedance of the 10 ohm line. One of the load resistors was tapped and used as the load voltage monitor. Both the target electrode and the load electrode have semielliptical heads with a diameter of 24 inches. The radius of a 24 inch in diameter semielliptical head is about 22 inches, which allows for the electric field at the axis of the electrodes to be within 5 percent of that of a plane parallel gap. The corners of the elliptical heads that would normally be regions of high field strength are, in this geometry, electrically shielded by the large diameter coaxial line conductors.

The six inches in diameter center portion of the electrodes could be removed for modification and inspection. The load electrode center portion features a 1/2 inch diameter opening through which the laser beam was allowed to pass. The entire load area can be pressurized with a dielectric gas in order to avoid corona losses. SF_6, at atmospheric pressure, was used in this region. Figures 8 and 9 show the target and load electrode respectively.

Diagnostic Equipment

The diagnostic equipment can be divided into three major categories: laser monitoring, pulser monitors and auxiliary equipment.

Laser Monitors

Three quantities relative to the laser pulse are of interest in this experiment. These are the laser pulse shape, the energy contained

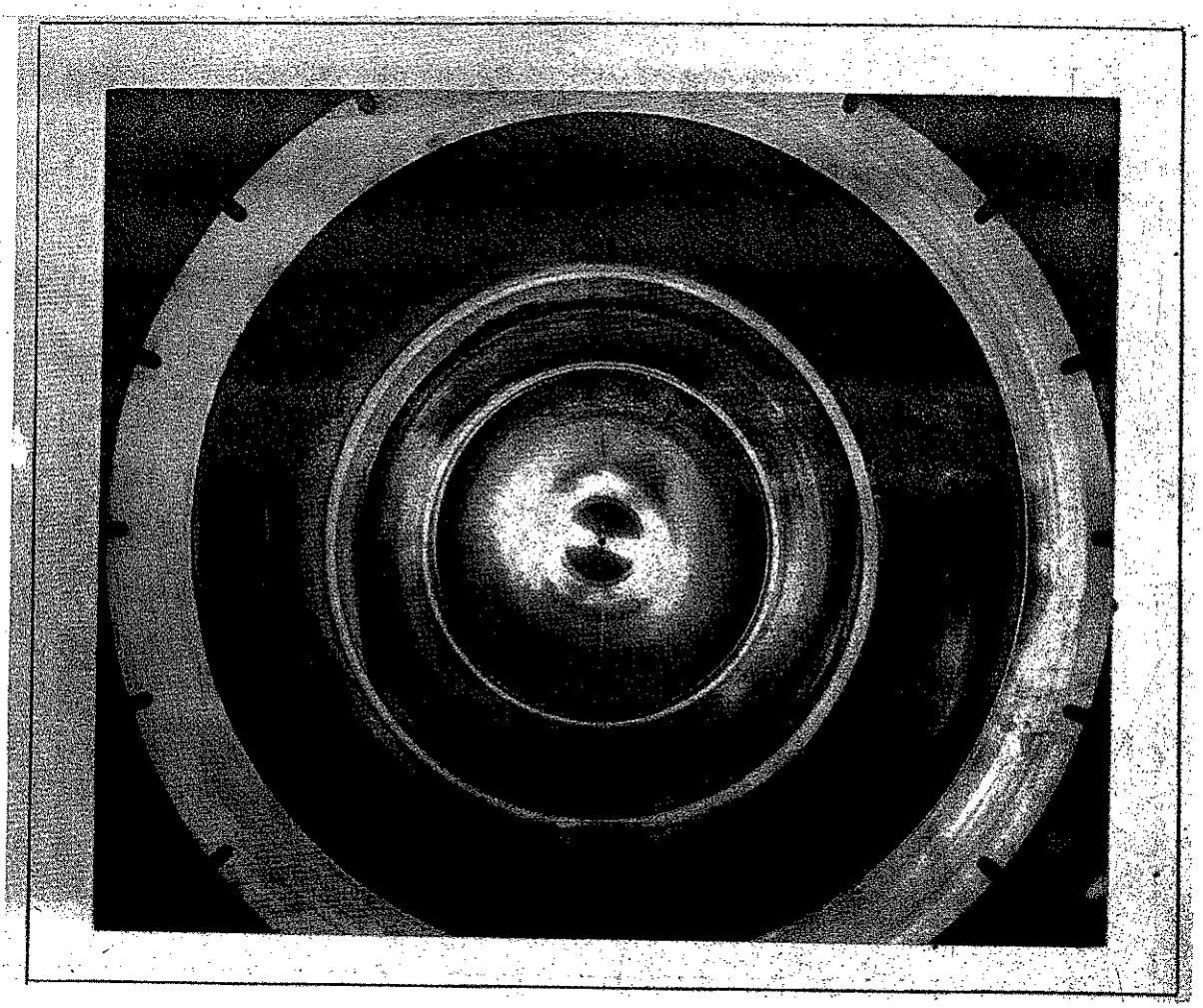

Fig. 8 Load Electrode Viewed Head-On

in the laser pulse and the time at which the laser pulse occurred. All these quantities were obtained by diverting a small portion of the beam into two sensors via the use of beam splitters.

The laser pulse shape and time reference was obtained by a S-20 ITT vacuum planar photodiode exhibiting a 0.1 nanosecond risetime. This output was monitored on a Techtronix 519 oscilloscope and divided for triggering other scopes as an initial time reference.

The laser pulse energy was monitored by a thin-foil calorimeter (foilometer) which consists essentially of a piece of aluminum foil to which a thermocouple has been attached. The foilometer was calibrated

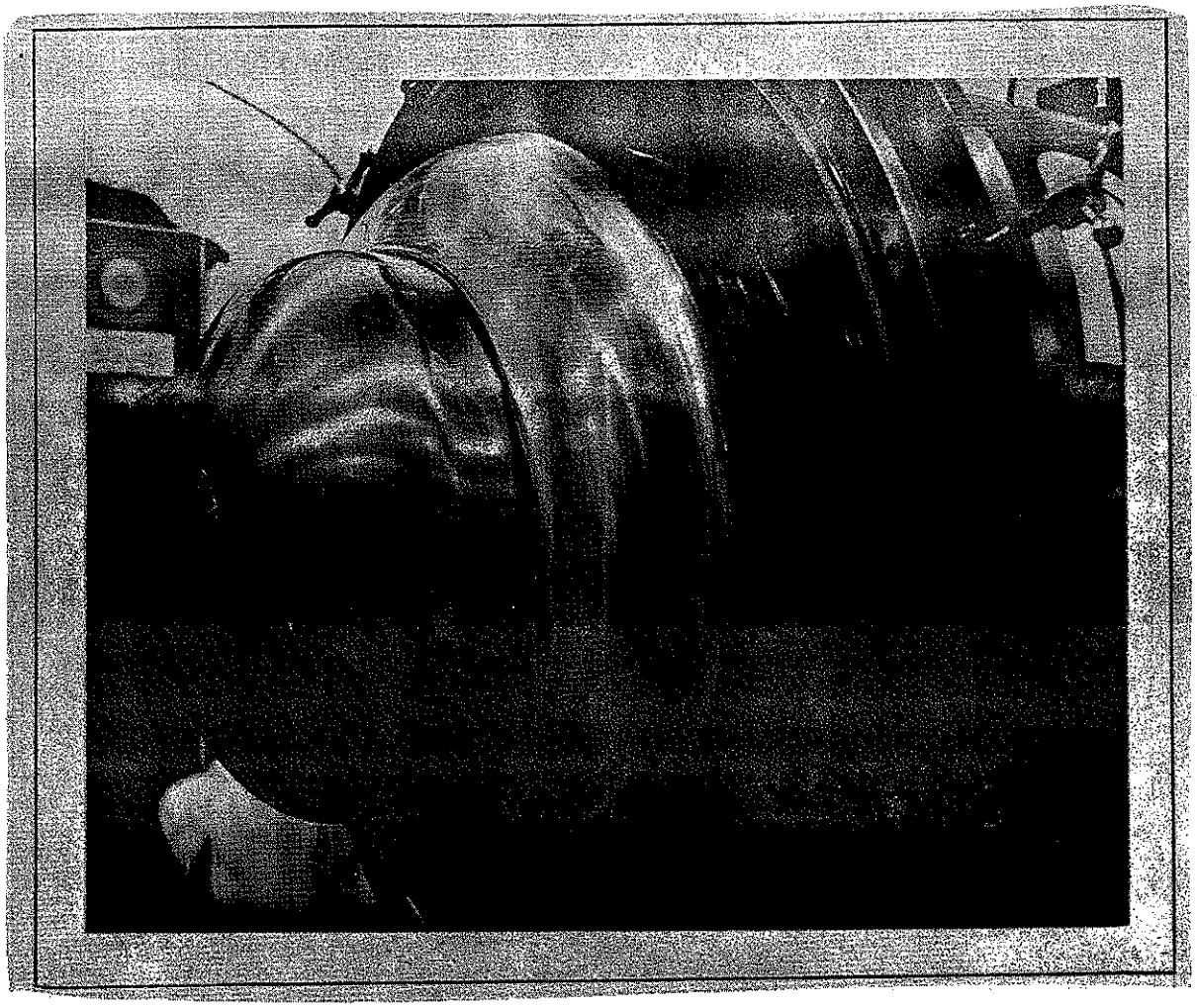

Fig. 9 Target Electrode

by simultaneously monitoring the foilometer and the total energy output of the laser system, the latter determined by a factory calibrated TRG Model 117 Thermopile. The signal of the foilometer was monitored on a Hewlet-Packard Model 425AR DC microvoltmeter and recorded on a Sanborn Model 7701A heated-stylus strip chart recorcer.

2 Mv Pulser Voltage Monitors

Two voltage monitors were used. One monitored the voltage pulse on the 10 ohm line whereas the other monitored the voltage across the load. The 10 ohm line voltage monitor employed a capacitive voltage divider network followed by a resistive divider network. The total

attenuation was 1500: 1 with a time constant of 30 microseconds which insures a deviation of less than 5% at 500 nsec from initiation of the voltage pulse. The load voltage monitor consisted of a resistive voltage divider network, tapped off one of the copper sulfate load resistors, followed by another resistive voltage divider. This last monitor was not calibrated as it was used strictly as a timing monitor for this experiment.

The two voltage monitors induced signals with peak amplitude of approximately 80 volts into the cables which insured a high signal-to-noise level. These signals were further attenuated at the inputs to the oscilloscopes where they were displayed. The line voltage was displayed on a Tektronix 555 dual beam oscilloscope simultaneously with the incident laser pulse and the load voltage was displayed on two Tektronix 519 oscilloscopes at two different sweep speeds.

Auxiliary Equipment

Electrical time delays of the coaxial line cables were measured with a Hewlett-Packard Time Domain Reflectometer with an accuracy of 0.1 nsec at the 20 nsec/cm rate.

The oscilloscope trace photographs were read on a Carl Zeis Model 1047 film reader with a reproducibility of $\pm$ 1.0 microns.

IV. Experimental Arrangement

This chapter will explain the reasoning behind the configuration used in this experiment and the problems encountered with the equipment. Also, a detailed explanation of the sequence of events that take place once the command signal is given to the system will be explained. The first section concerns itself with the high noise levels encountered in this experiment and the methods used to overcome them. The second section describes the sequence of events while the last section describes the problems encountered with the equipment degradation. In Fig. 10 a detailed layout of the total system is presented as reference for what follows.

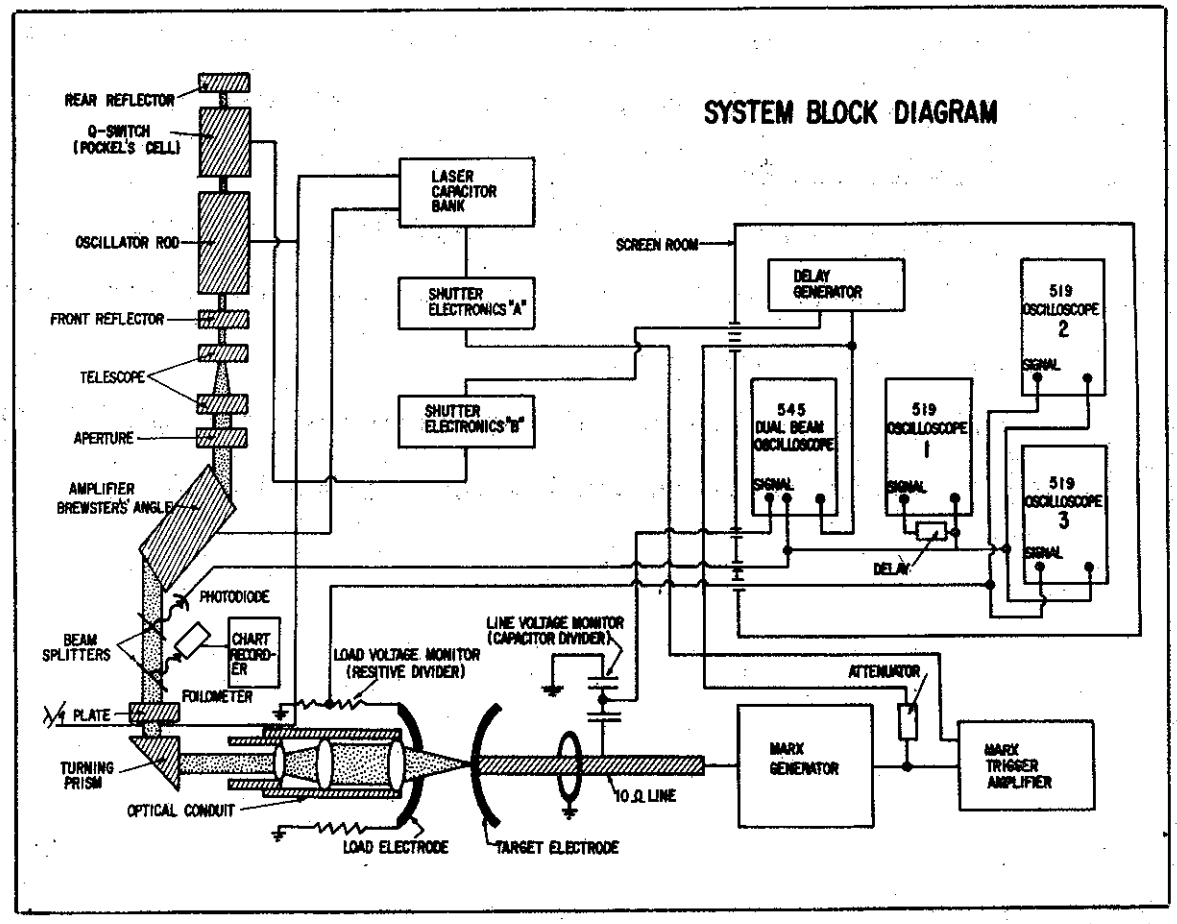

Fig. 10 Detailed LTS System Block Diagram

Induced Noise

High noise levels were generated in the area surrounding the entire system. These high noise levels, generated by the high electromagnetic fields produced during the discharge of the laser capacitor banks and the erection of the Marx generator, were capable of inducing voltage pulses on the order of six volts in solid shield, well grounded coaxial cables. The major effect of this induced noise was twofold. First, it presented serious problems with the oscilloscopes and delay generators causing them to trigger before the real triggering signal arrived. This problem of pre-triggering was solved by raising the triggering voltages and using Zener diodes to block the induced noise. The second problem was the erratic behavior of the oscilloscope traces in the presence of high EM fields. This problem was solved by placing all the oscilloscopes and the delay generator inside a double shielded 120 db attenuation RF screen room.

Sequence of Events

The first consideration that had to be given to the connection of the laser system to the 2 Mv pulser was the selection of a zero-reference time from where the sequence of events that followed for the two systems would be independent of each other. This reference point will determine the reproducibility of the timing of the laser to a particular point on the voltage ramp. This accuracy, or jitter, will be the sum of the jitter associated with the voltage pulse and the jitter of the laser pulse, both taken with respect to the reference point. Due to the nature of the laser system used, which requires a minimum of 480 nsec between the input of shutter electronics B and the onset of lasing, this experiment had to settle for the Marx trigger amplifier

output as the zero-reference time. This selection allowed a jitter of 65 nsec between the reference point and the delay of the laser arrival at the target electrode (15 nsec due to the laser and 50 nsec due to the Marx generator). A discussion of how this overall jitter can be reduced will be found under recommendations.

The slowest element dictated where the trigger signal should be picked off from, after this element had been activated. This slowest element or event was determined to be the occurrence of the optimum population inversion in the laser ruby rods, an event that requires approximately 1.1 milliseconds to occur after the flashlamps of the laser had been activated. The sequence of events then starts off with the discharging of the capacitor banks into the laser flashlamps. This sequence of events can be followed with the assistance of Fig. 11, the system's electrical circuit.

The discharging of the laser capacitor banks into the flashlamps is sensed by a di/dt loop, whose signal is fed into shutter electronics A where it is delayed by approximately 1.17 milliseconds. The output of shutter electronics A is allowed to trigger the Marx trigger amplifier, then taking approximately 500 microseconds to appear at its output.

Since the output of the Marx trigger amplifier is zero-time, all the succeeding events and their times will be given with respect to this output. At 64.7 nsec the high voltage monitor signal of the Marx trigger amplifier output arrives at the laser delay generator. Insertion of the desired delay into this delay generator will permit the laser pulse to arrive at different voltages on the target electrode. An output is taken from the delay generator and at 398.7 nsec triggers

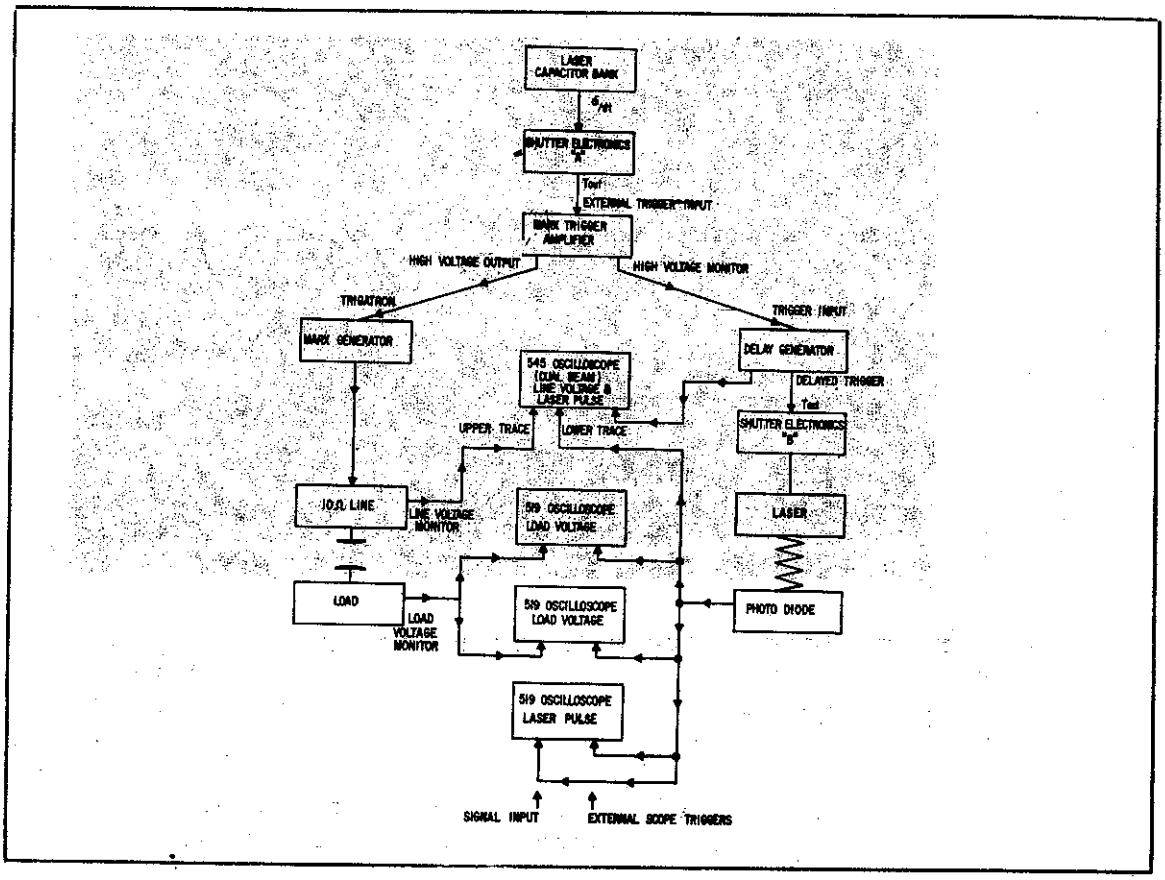

Fig. 11 LTS System Trigger and Signal Flow Chart

the 555 dual beam oscilloscope. At (128.9 + delay) nsec, electronic shutter B receives the triggering signal which results in lasing at (608.1 + delay) nsec, an event which is sensed by the photodiode. At (656.1 + delay) nsec, the laser pulse appears on the signal input of the lower trace of the 555 dual beam scope while at (745 $\pm$ 50) nsec the signal from the 2 Mv pulser line voltage monitor is displayed on the upper trace of this dual beam oscilloscope. Figure 12 shows a typical trace obtained from the 555 dual beam oscilloscope.

At (651.1 + delay) nsec and at (656.1 + delay) nsec the two 519 oscilloscopes used to display the load voltage monitor signal are triggered by the laser pulse. The load voltage monitor signal was displayed simultaneously on both oscilloscopes at breakdown plus 60.0

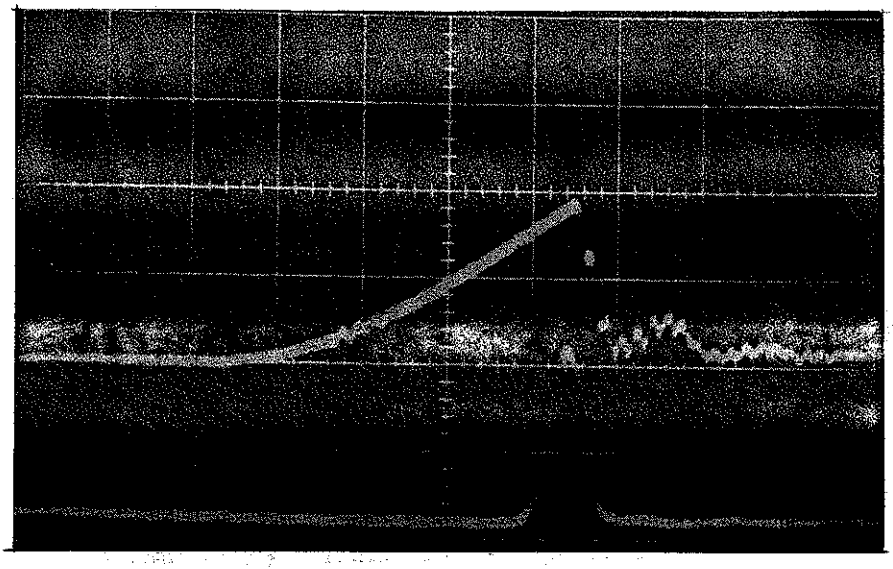

Upper Trace: Line Voltage Monitor
Attnn: 300kV/cm
Sweep: 100nsec/cm
Trigger: Marx Trig Amp

Lower Trace: Laser Pulse
Attnn: Relative
Sweep: 100nsec/cm
Trigger: Marx Trig Amp

Fig. 12 555 Dual Beam Oscilloscope Trace:
Line Voltage Monitor and Laser Pulse

nsec. The first scope was used with its sweep rate set at 20 nsec/cm whereas the latter was set at 100 nsec/cm. Typical traces obtained from these two scopes are shown in Figs. 13 and 14.

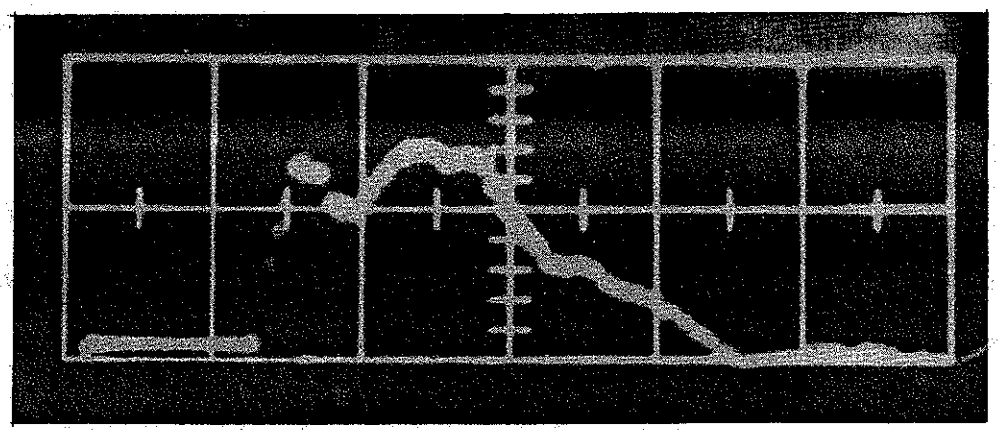

Trace: Load Voltage Monitor
Attnn: Relative
Sweep: 20nsec/cm
Trigger: Laser Pulse

Fig. 13 519 Oscilloscope Trace:
Load Voltage Monitor - Fast Sweep

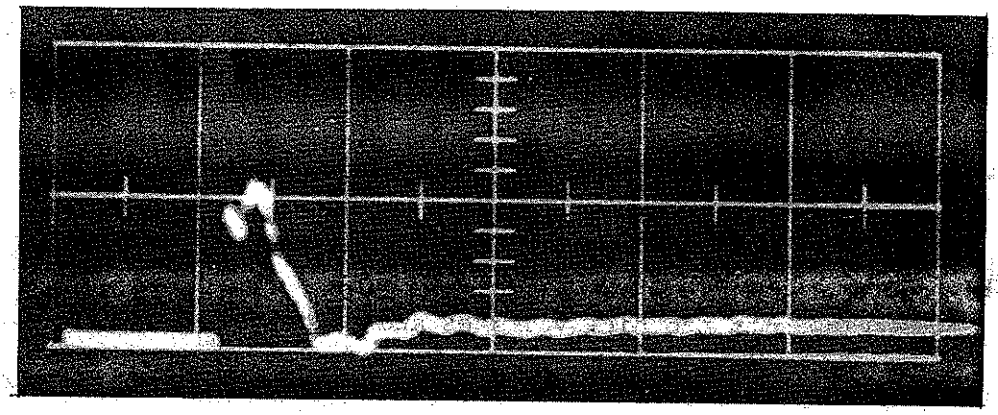

Trace: Load Voltage Monitor
Attnn: Relative
Sweep: 100nsec/cm
Trigger: Laser Pulse

Fig. 14 519 Oscilloscope Trace:
Load Voltage Monitor - Slow Sweep

Finally, at (689.1 + delay) nsec the 519 oscilloscope displaying the laser pulse is triggered by the laser pulse which itself is displayed 20 nsec later, as exhibited in Fig. 15.

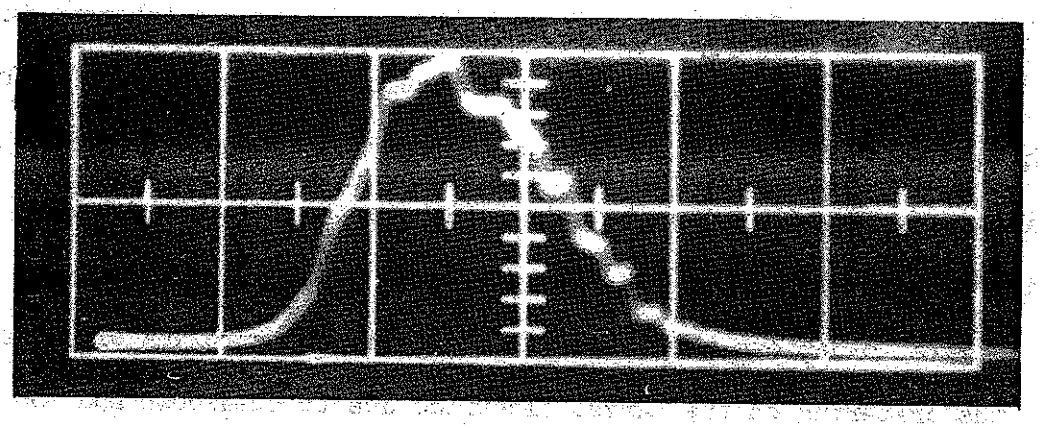

Trace: Laser Pulse
Attnn: Relative
Sweep: 20 nsec/cm
Trigger: Laser Pulse

Fig. 15 519 Oscilloscope Trace:
Laser Pulse Monitor

The last important timing parameter is the time of flight of the laser pulse between the photodiode and the target electrode. This time was calculated to be 6.46 nsec since the two elements are separated by 75 inches.

Equipment Degradation

On working with the high voltages and high laser power densities encountered in this experiment, consideration must be given to the equipment degradation for future systems employing the LTS technique in liquid dielectrics. This discussion will be divided among the three main components of this system.

2 Mv Pulser Degradation

The main area of degradation of the 2 Mv pulser occurred to the electrodes and dielectric in the switch chamber. There also exists a slower degradation of the Marx generator and the 10 ohm line due to carbon buildup along the insulating supports in the high field regions. The mid-plane gaps connecting the Marx stages also exhibited deterioration after about 300 shots. These latter problems are inherent in any pulse generating system and do not particularly relate to the LTS technique. The first two areas, the dielectric and the electrodes, are of importance for they can strongly influence the parameters of the entire system.

Figure 16 depicts the target electrode after approximately 60 shots. Note the cratering on the target electrode due to breakdown and the dispersion of these craters with a high concentration along the approximate center of the target. The craters have two distinct regions; a highly circular center portion which can be accounted for by laser

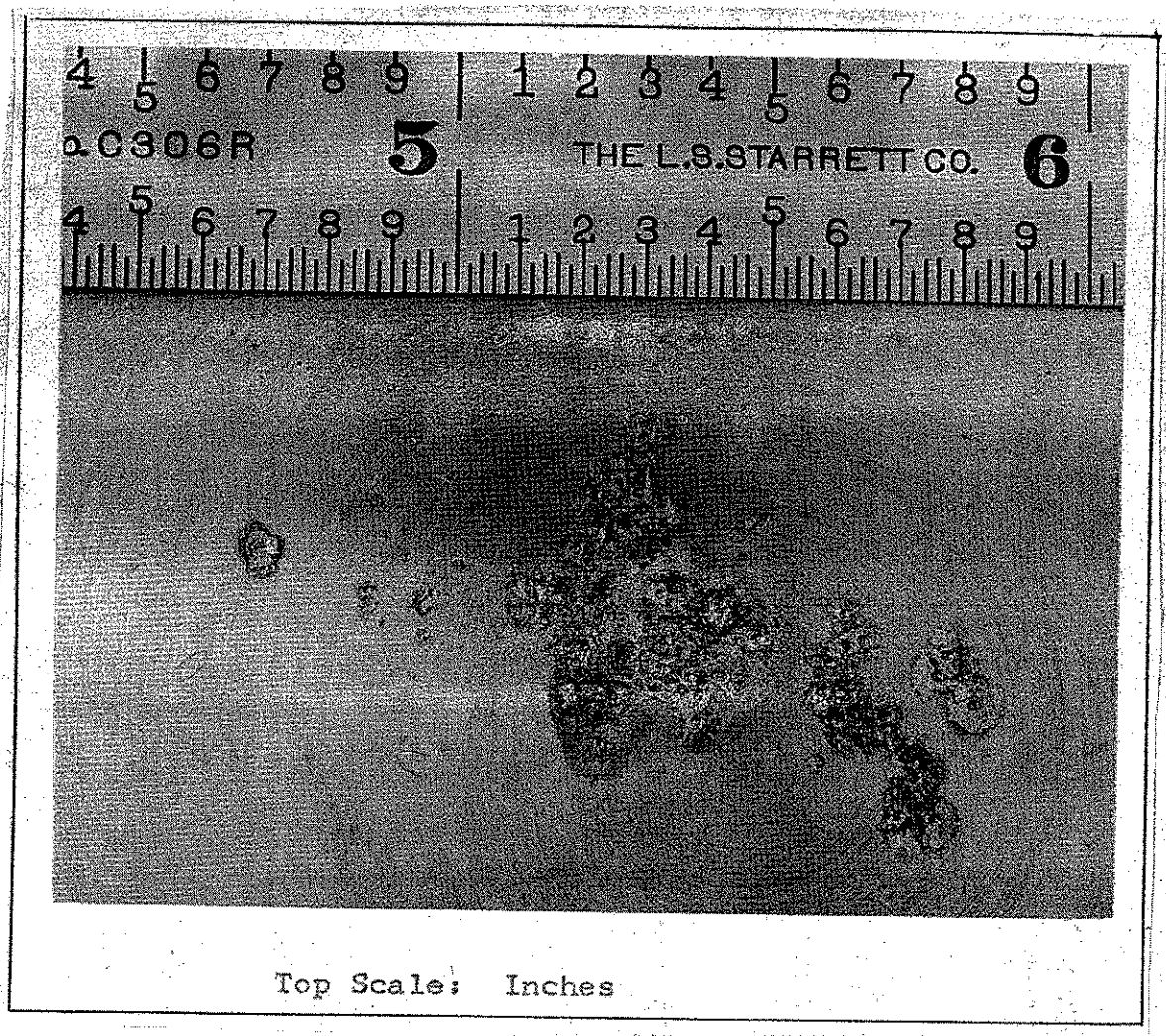

Fig. 16 Target Electrode Condition
After 60 Shots

vaporization of the target material and a more irregular outer portion that can be accounted for by the breakdown itself. These same irregular circular craters appear in the load electrode. Some dispersion of the craters can be accounted for due to the misalignment of the laser beam with the optical axis of the lens system and by the self-breakdown. Approximately 15 alignment sequences took place during the 60 shots due to the mechanical failure of the +2 inch focal length lens. The alignment procedure left much to be desired as to the

accuracy and should be simplified or improved.

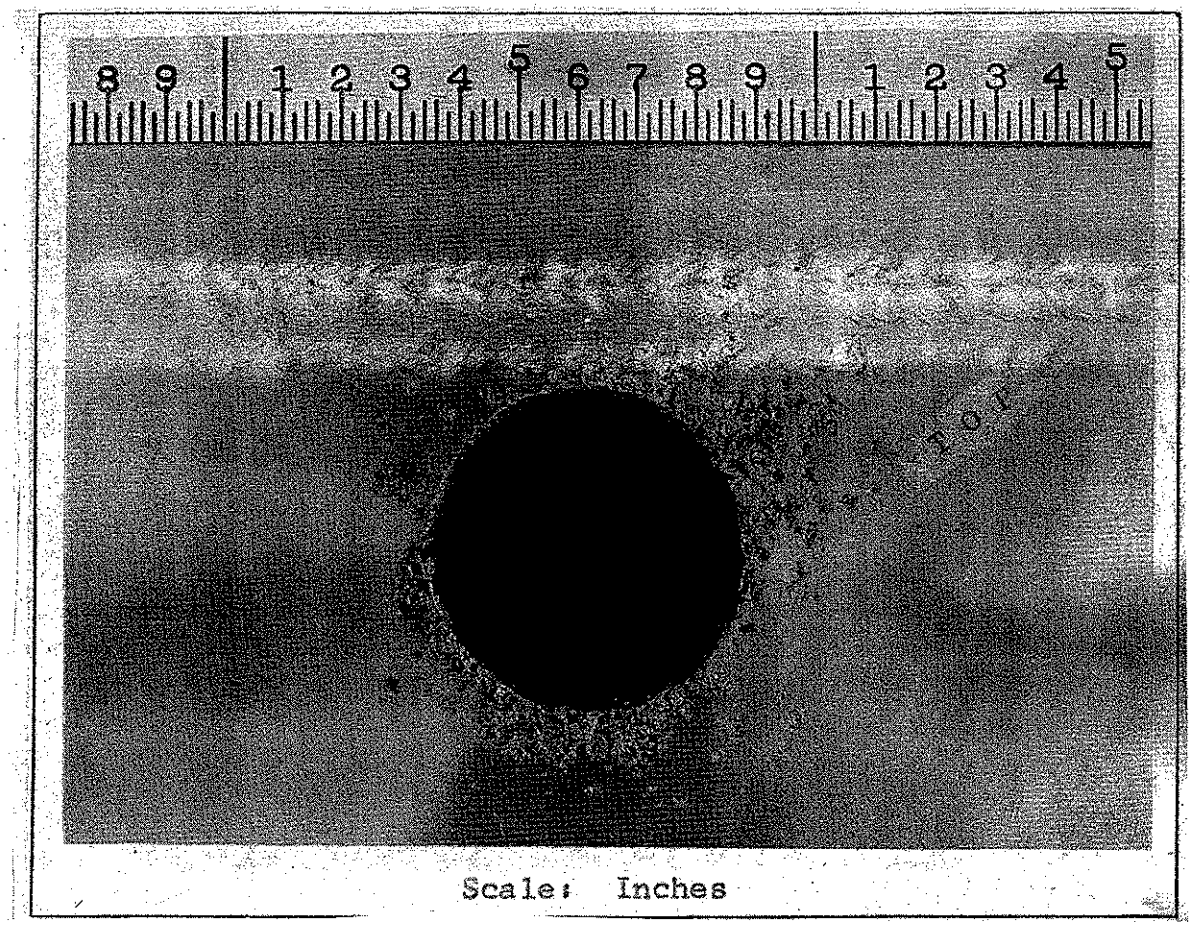

Fig. 17 Load Electrode Condition After 60 Shots

The load electrode is depicted in Fig. 17, again, after 60 shots. The important observation to be made is the strong degradation of the border of the $\frac{1}{2}$ inch laser port. This concentration of craters is due to higher field regions present near the border of the aperture with respect to the surface of electrode. Note the unusually high concentration of craters along the top of the laser port opening. This is probably due to the presence of minute air bubbles generated by the +2 inch focal length lens cleaning assembly which circulated the switch area dielectric over this final lens. Note also, the irregular

circular craters similar to the ones on the target electrodes produced by the breakdown. No highly circular craters can be observed in the center of these craters.

The dielectric used, transformer oil, carbonized along the path of breakdown. No quantitative measurements were made to determine the products of this carbonization. To eliminate the carbon path, the dielectric was recirculated and removed by the turbulence of the recirculation. Approximately every ten shots the dielectric was pumped back to the main reservoir and mixed with the rest of the dielectric. The switch chamber was then refilled from this reservoir. It should be noted that the variation between the DC breakdown voltage tests conducted before and after the conclusion of the experiment were within one percent.

Optical System Degradation

The main problem area of the system was the mechanical failure of +2 inch focal length lens. This lens was placed three inches from the load electode and had the oil dielectric on one side and air on the other. This lens would break after an average of five to six LTS shots. The cause for the failure of the lens was a combination of the high laser power densities and the shock produced by the breakdown. This breakdown shock was coupled by the relatively incompressible liquid dielectric to the face of the lens. This same lens held up to the breakdown shock of self-breakdown (no laser used) and showed no laser damage or pitting if the laser alone was used. Figure 18 depicts a sequence of failure. Starting with the upper right hand corner and going counterclockwise, the lens appears with a slight crack and grows with further LTS shots to final total mechanical failure.

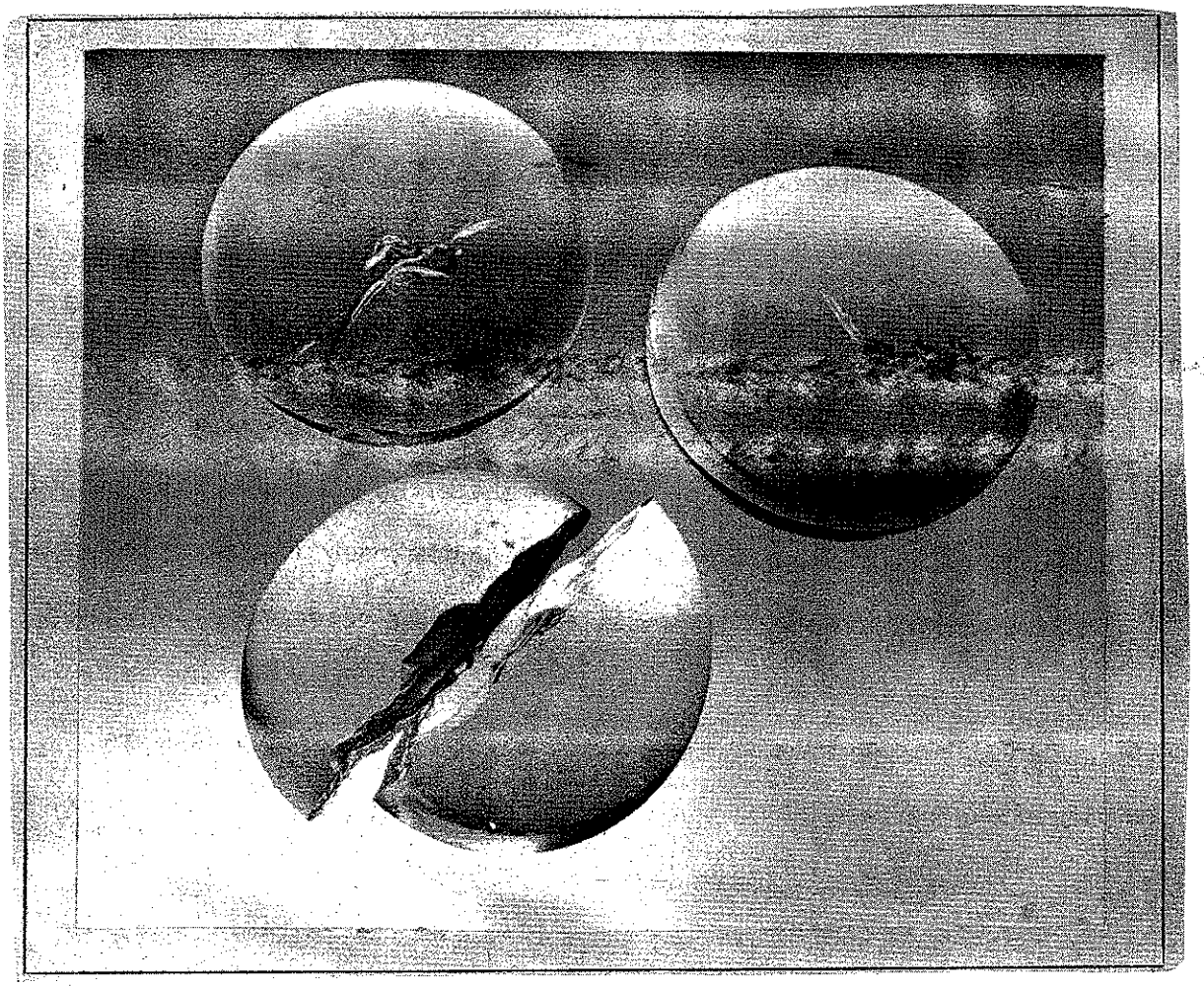

Fig. 18 +2 inch Focal Length Lens Breakage

LTS causes a linear channel (see Fig. 20) which propagates along the optical axis from the target electrode to the load electrode. Hence hydrodynamic loading is most severe when considerable electrical energy is deposited along the laser generated breakdown channel. Note that during self-breakdown (see Fig. 19) the hydrodynamic shock is of random nature due to the branches of the breakdown paths.

Several attempts were made to correct this problem but they all failed. These attempts included the placing of a 3/4 inch thick quartz plate between the load electrode and the lens, but the plate broke after the first LTS shot. A smaller diameter +2 inch f lens

was tried, but the 1/4 inch plexiglass support broke after a few shots resulting in the support and the lens being propelled along the tube and causing the breakage of the middle lens. The experiment was conducted by examining the lens after every shot and substituting the lens whenever it appeared to be cracked. A total of 35 lenses were damaged during the 140 shots taken for this experiment.

Towards the end of the experiment the optical conduit was fractured due to the shock of LTS induced breakdown. It was replaced and a second one broke after 30 shots. It should be noted that while these breakdown events also occur in the LTS of gases, they do not support a strong coupling of the shock as well as the liquids because of their increased compressibility.

Laser System Degradation

Three oscillator rods exhibited very short lifetimes in the laser system before the cause of this lifetime reduction was determined. This mechanism was determined to be a stimulated Brillouin scattering from the liquid dielectric.

The reflection was determined to be from the dielectric by careful analysis of the laser pulse waveform. It was noted that the laser pulse exhibited two peaks when the pulse was allowed to enter the transformer oil whereas the second peak was not present if the optical port was covered. The second peak was determined to be approximately 25 nsec from the start of the laser pulse and bore a strong resemblance to the initial laser pulse itself. The strong resemblance led to the conclusion that it must be some form of reflection being amplified by the laser system, back through the amplifier rod to the oscillator rod. The time of flight of 25 nsec indicates a travel path by the laser

pulse of about 294 inches. This path represents the roundtrip distance between the photodiode, the reflection, the rear reflector of the oscillator cavity and back to the photodiode. Hence, the next step was to investigate where a reflection could occur that was about 147 inches from the rear reflector of the oscillator cavity. Only the distance to the dielectric in the switch chamber exhibited such length. For a maximum enhancement this reflection should be of the same polarization of the laser beam, for otherwise the returning reflection would be partially reflected at the face of the amplifier rod (the face of the amplifier rod is cut at Brewster's angle). Stimulated Brillouin scattering-off of the dielectric in the switch chamber met all the above mentioned conditions.

The 180° stimulated Brillouin scattering is basically a reflection at a boundary where a change of index of refraction occurs. This change of index of refraction is caused by thermal and pressure waves travelling at random directions throughout the liquid. These reflections are compounded by the laser which selects the reflections that meet Bragg's law of reflection and produce a sort of constructive interference of the reflections. These reflections are of the same polarization as the incident laser beam and slightly shifted up and down in frequency from that of the laser. These reflections, which can be as much as 80% of the incident power (Ref. 23), pass through the optical system and impinge on the amplifier rod. Being of the same polarization of the outgoing light, the reflection is allowed to go through the amplifier rod where an appreciable population inversion is present. The stimulated Brillouin scattering is still within the flourescent line width of the laser but slightly shifted from its initial frequency due to Doppler

effect. The reflection can then cause stimulated emission of the inverted population and thus be amplified. The amplified reflection is then concentrated by the Galilean telescope between the amplifier and oscillator rod and strikes the face of the oscillator rod. It is then further amplified in the ruby rod by the same process described for the amplifier rod. The oscillator rod is then subject to radiation power levels where any minor flaw in the ruby rod, that would normally not cause any concern, becomes a center where damage to the ruby crystal lattice can occur.

The Brillouin reflection was partially eliminated by using a Brewster's plate polarizing tent and a 6943A° quarter wave retardation plate. This assembly operates in the following manner. The horizontal radiation from the output of the laser, which is incompletely polarized, passes through the Brewster stack tent to purify its polarized nature with an optical attenuation of less than 5%. It is then rotated by 45° in polarization by the quarter wave retardation plate. The stimulated Brillouin scattering, which returns on axis with the same polarization as the incident light, is then further rotated by the quarter wave plate by another 45°. The resulting vertically polarized light is then rejected by the Brewster tent. By using this simple Brillouin reflection rejection system the lifetime of the oscillator rods was greatly increased and no more double pulsing was observed.

V. Data Analysis

This chapter will first define the parameters affecting this experiment and explain how they were obtained and cross checked. The results obtained will be then given in graphical form using the delay to breakdown to compare the effect of each parameter. A brief explanation of the graphs will also be found in this chapter. The first section deals with the definition, followed by the section describing how the determination of each parameter was accomplished. The third section presents the data.

Parameter Definition

The main parameters monitored in this experiment were: gap spacing, laser focal point position, laser energy, laser power, delay to breakdown, delay to laser arrival, voltage and polarity on target electrode at laser arrival, and breakdown voltage.

Other secondary parameters, such as pressure of the SF_6 on the Marx generator mid-plane gaps, air pressure of the trigatron of the Marx generator, dielectric condition, optical system condition and electrode condition were monitored on every shot to verify that they were at the nominal values or conditions.

Gap spacing is defined as the distance of minimum separation between the two electrodes. Laser focal point position is defined as the position of the most forward plasma formation present in the experimental determination of the focal position. The laser focal point position is measured relative to the load electrode. Laser energy is defined as the total energy present in the giant pulse produced by the laser. Laser power is defined as the peak instantaneous power achieved by the giant pulse of the laser. Delay to breakdown is defined as the

time between the laser arrival at the target electrode and the conduction of the gap. Delay to laser arrival is defined as the time between the start of the voltage pulse on the target electrode and the arrival of the laser at the target electrode. Voltage on target electrode at laser arrival is defined to be the instantaneous voltage on the target electrode at laser arrival. Breakdown voltage is defined to be the instantaneous voltage on the target electrode at the initiation of conduction of the gap.

Data Reduction

The following section will explain how the data was obtained and reduced.

Gap Spacing: The gap spacing was determined by a thickness gauge block made out of aluminum. This gauge was inserted from the top of the switch chamber and the target electrode adjusted to its proper location. A cathetometer was used as a cross check for the first few adjustments.

Laser Focal Position: The laser focal position was first calculated theoretically as shown in Appendix A. An experimental curve was determined by opening the gap spacing to its fullest extent and firing the laser into the switch chamber without erecting the Marx generator. The laser focal position was varied by adjusting the telescope and time integrated photographs were taken of the laser breakdown of the dielectric in the switch chamber. By using the gap spacing, determined by using the cathetometer, as a scale factor, one can convert the most forward plasma formation of the laser breakdown of the dielectric to the actual distance from the load electrode.

Laser Energy: Laser energy was read out directly from the calibrated Sanborn strip chart recorder, as described under laser diagnostic equipment.

Laser Power: Laser power was determined from the laser pulse waveform and the laser energy. The full width at half maximum (FWHM) of the laser pulse is obtained from the laser pulse waveform. Assuming that the laser power curve, as a function of time, closely approximates a Gaussian distribution, one can divide the laser energy by the FWHM in nanoseconds and obtain the peak laser power.

Delay to Breakdown: The delay to breakdown was obtained from three experimental measurements and cross checked analytically. The experimental values were obtained from the 555 dual beam oscilloscope and the two 519 oscilloscopes monitoring the load voltage. The delay to breakdown is taken from the 555 oscilloscope by measuring the difference in time between the start of the laser pulse and the conduction of the gap, the latter seen as a sharp drop on the line voltage monitor signature. The other two experimental values are taken from the 519 scopes by simply measuring the time between the start of the trace and the start of the rise of the load voltage. All three values take into account the cable lengths and time of flight of the laser. The last two experimental values assume that the difference in time for the target electrode to "notice" the initiation of the conduction and the load electrode to register the increase voltage is negligible. The analytical cross check was made by using the delay to laser arrival and adding the delay to breakdown. This total time was then used to determine the voltage at which the gap broke down from the voltage pulse waveform.

This determined breakdown voltage was compared to the experimentally determined breakdown voltage. All three values were within 5.5 nsec of each other and the two breakdown voltages compared within 5% of each other.

Delay to Laser Arrival: The delay to laser arrival was determined from the two traces of the 555 dual beam oscilloscope. This value was directly read from the trace as the time difference between the start of the voltage pulse on the target electrode and the start of the laser pulse, taking into account the laser time of flight and the difference in cable lengths. This value was cross checked analytically by using the voltage waveform and determining the voltage at the target electrode on laser arrival. The analytical value and the experimental value of the voltage on the target electrode at laser arrival compared favorably and were within the 5% error associated with the line voltage monitor.

Voltage on Target Electrode at Laser Arrival: The voltage on the target electrode at laser arrival was determined by reading the voltage on the target electrode directly off the top trace of the dual beam 555 oscilloscope at the start of the voltage pulse. The value of the voltage on the target electrode at laser arrival is usually expressed in percent of the self-breakdown voltage.

Breakdown Voltage: The breakdown voltage was read directly from the top trace of the 555 dual beam scope as the maximum vertical deflection of the 10 ohm line voltage monitor.

Results

The results of this experiment will be presented in the form of

semi-logarithmic plots. The dependent variable will be the delay to breakdown in nanoseconds with the independent variable being the voltage on the target electrode at laser arrival expressed in percent of self-breakdown. One will note that the voltage on the target electrode is directly related to the delay to laser arrival.

The straight lines depicted are best fit lines using the minimum root mean square deviation. The root mean square deviations were calculated for each point by the assistance of a computer program found in Appendix C. The standard deviation of the slope of the line and the equation of the line were also computed. Finally, the breakdown voltage versus the voltage on the target electrode at laser arrival is shown in a linear plot.

Self-breakdown voltage of the negatively charged target electrode was found to be (600 $\pm$ 30) kv, while the positively charged target electrode was (700 $\pm$ 35) kv. Both were determined for a 20 mm gap. Figures 19 and 20 are time integrated photographs of the self-breakdown and LTS breakdown respectively. Note the straight breakdown when initiated by the laser versus the branched breakdown observed for self-breakdown.

Negative Target Electrode

Figure 21 depicts the delay to breakdown versus voltage on target electrode in percent of self-breakdown. Three important observations can be made from this plot. First, the plot of delay to breakdown for focus location of 22 mm and laser power from 120 to 170 Mw depicts two distinct slopes, with an inflection at a target voltage at laser arrival 30% of VSB. Second, the lower the laser power, the longer the delay to breakdown for the same focal position. Finally, the optimum

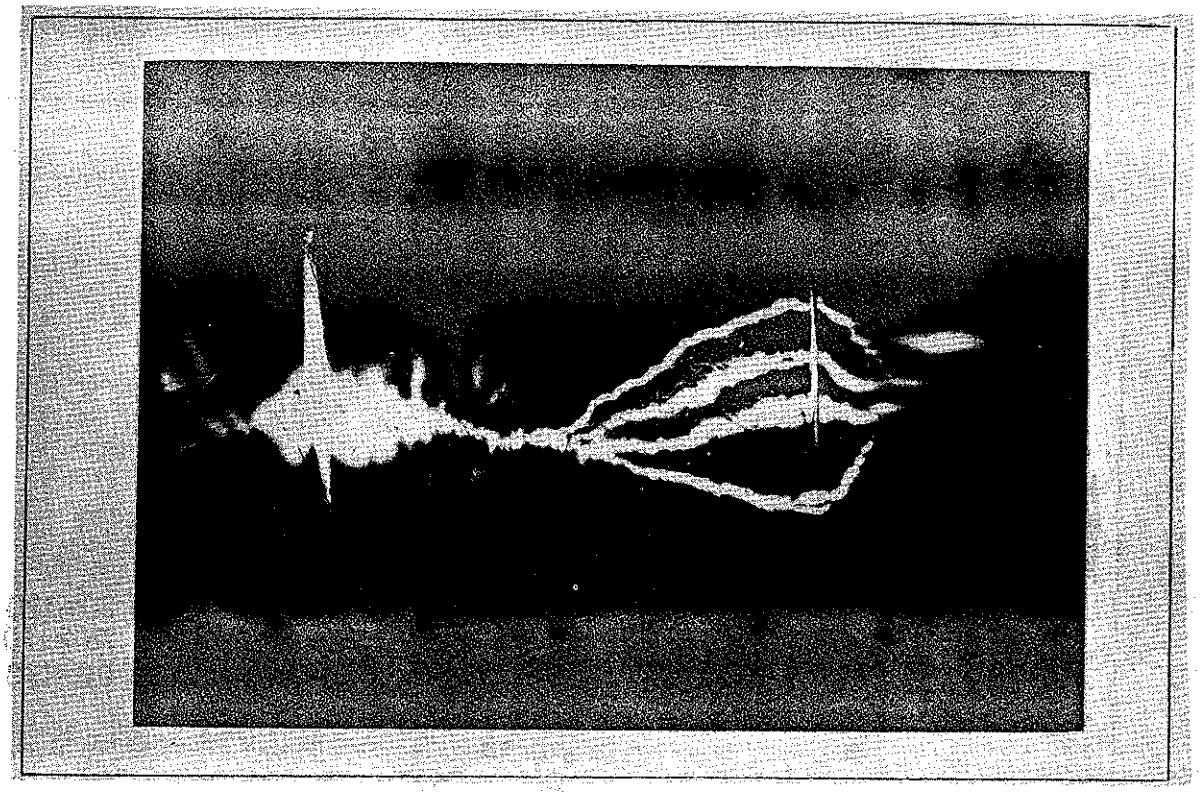

Fig. 19 Self-breakdown at 600 kv of a 20 mm Gap
(Left - Target Electrode; Right - Load Electrode)

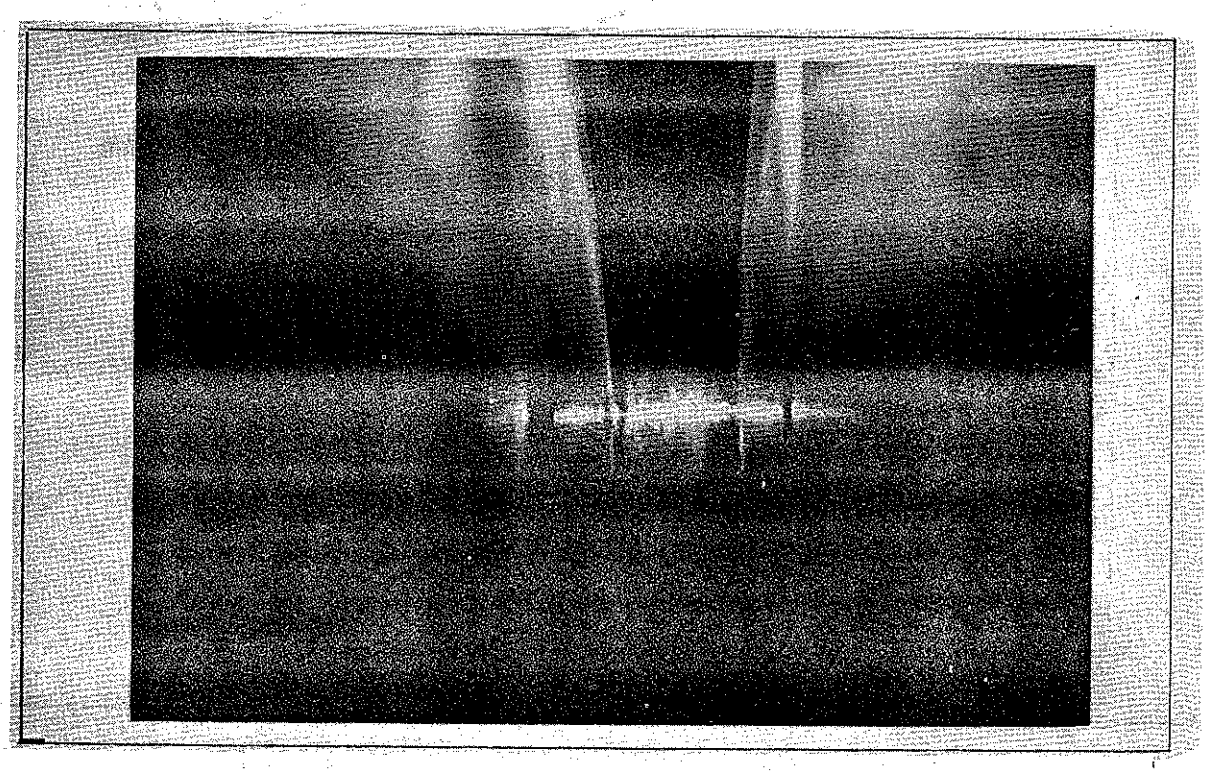

Fig. 20 LTS Breakdown at 580 kv of a 20 mm Gap Laser Travelling from Right (Load Electrode) to Left (Target Electrode)

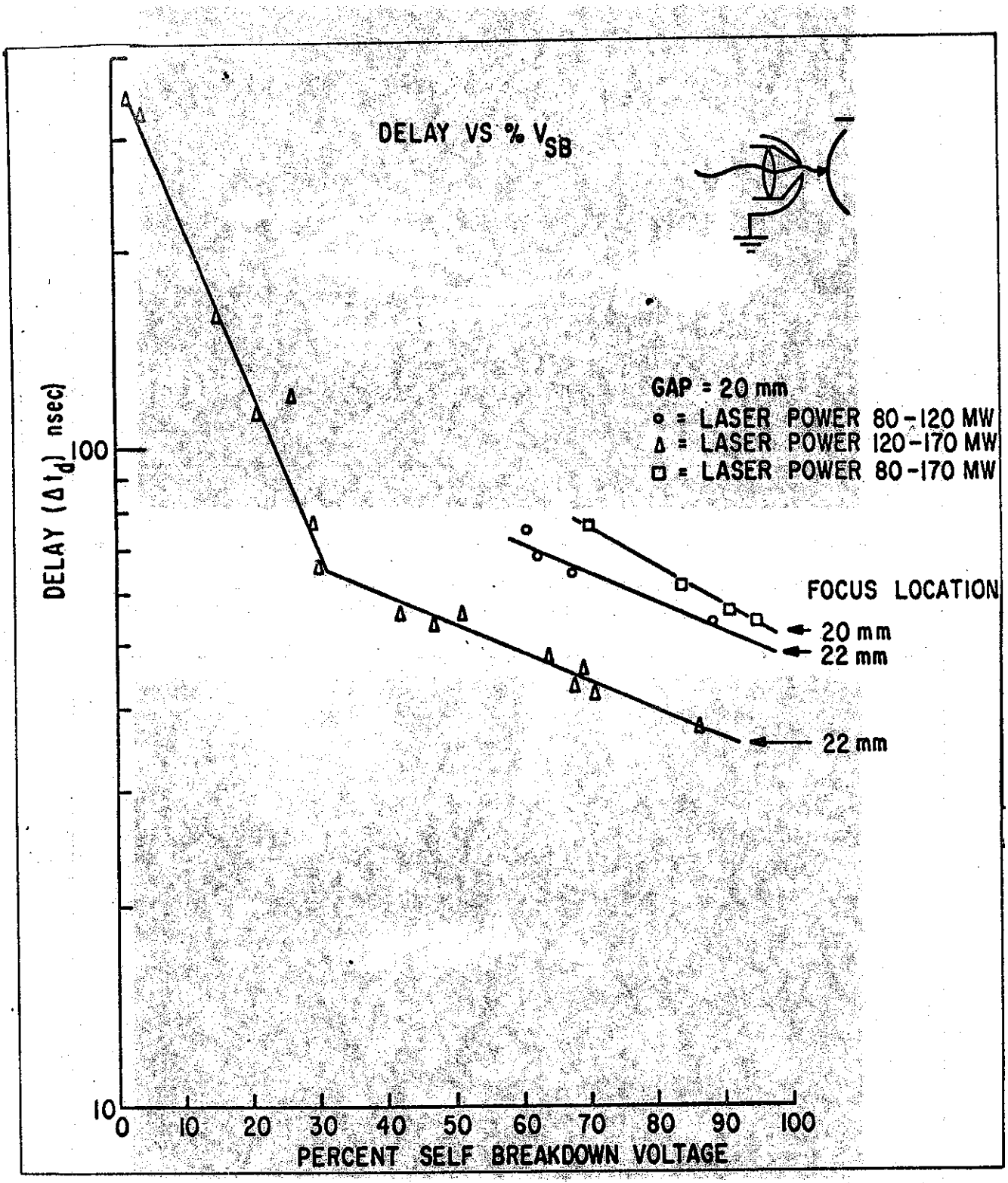

Fig. 21 Delay to Breakdown versus Voltage on Target Electrode at Laser Arrival - Negative T.E.

laser focus position was found to be at 2 mm inside the target electrode. Only the focal position of 20 mm is presented, but data points taken at a focal position of 27 mm from load electrode (7 mm inside the target electrode) also demonstrated higher delay to breakdown than that at 20 mm.

Figure 22 depicts the breakdown voltage versus voltage at laser arrival. The straight line of Y=X can be considered the zero delay to breakdown line. Note the bend on the RMS line joining the data points at a voltage at laser arrival 180 kv (30% self-breakdown).

Positive Target Electrode

Figure 23 depicts the delay to breakdown versus voltage on target electrode in percent of self-breakdown. Three important observations can be made from this plot. First, each of the lines for different focal positions and different laser powers present two distinct slopes. Second, the delays to breakdown associated with the higher laser powers of the 22 mm focal positions are shorter than the delays associated with the lower laser powers for the same focal position. Finally, the optimum focal position was found to be at 22 mm (2 mm inside the target electrode). Data was taken for a focal position of 14.5 mm from load electrode (5.5 mm in front of the target electrode) which exhibited longer delays than the ones taken at the 22 mm focal position.

Figure 24 depicts the breakdown voltage versus voltage on target electrode at laser arrival. Note that there seems to be a break in the slope of the lines joining the data points. This break point is less distinguishable than the one present for a negatively charged electrode.

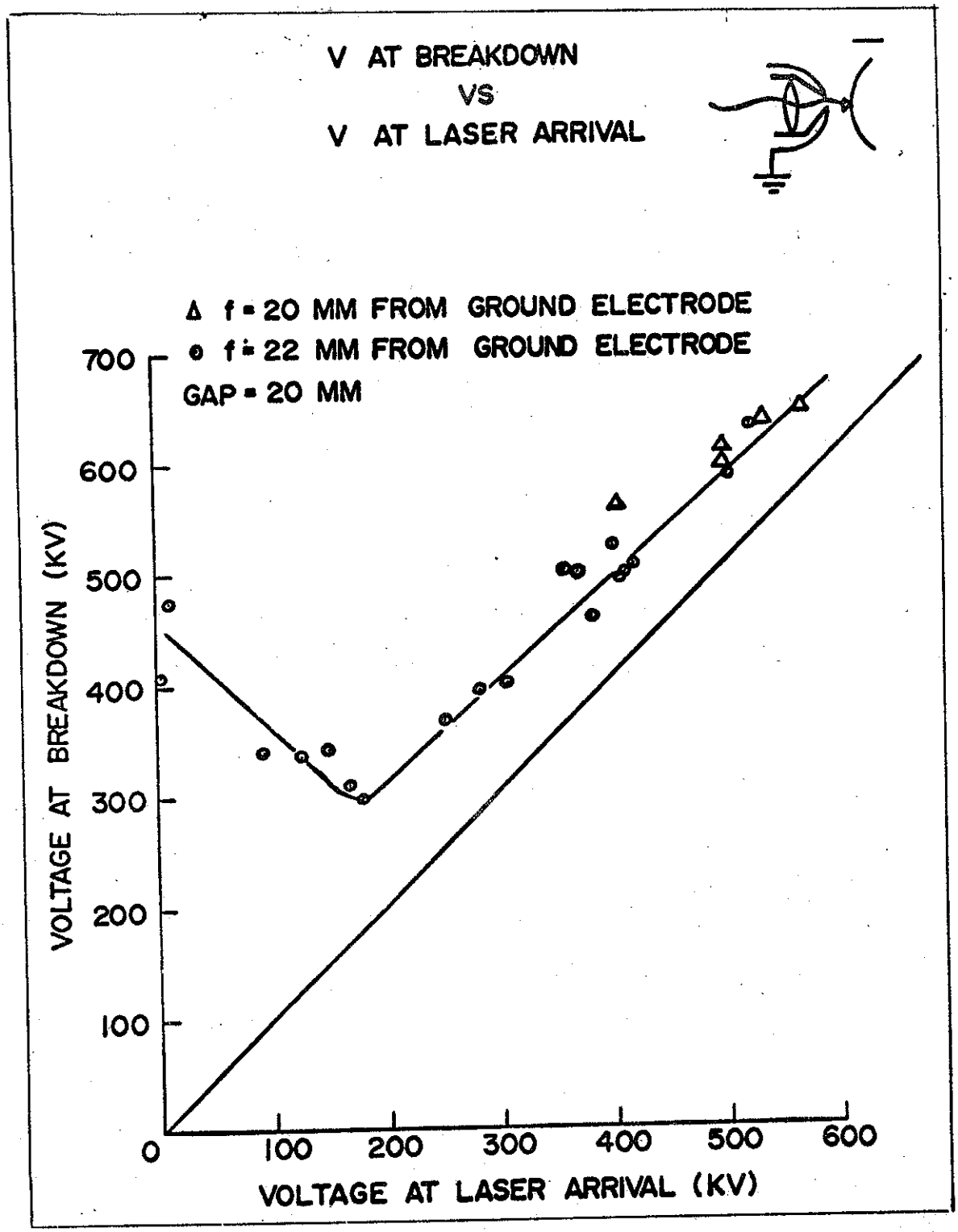

Fig. 22 Breakdown Voltage versus Voltage on Target Electrode at Laser Arrival - Negative T.E.

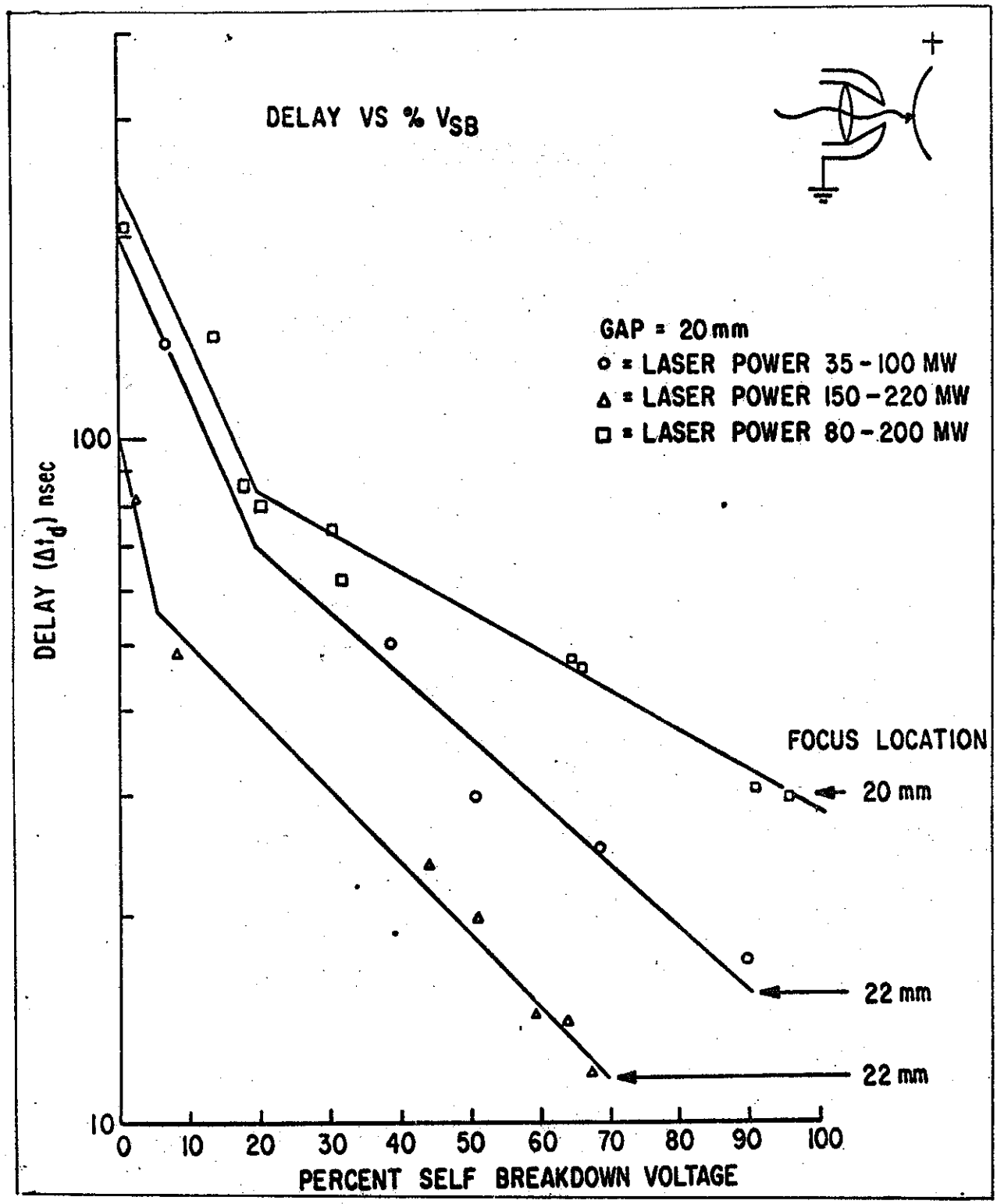

Fig. 23 Delay to Breakdown versus Voltage on Target Electrode at Laser Arrival - Positive T.E.

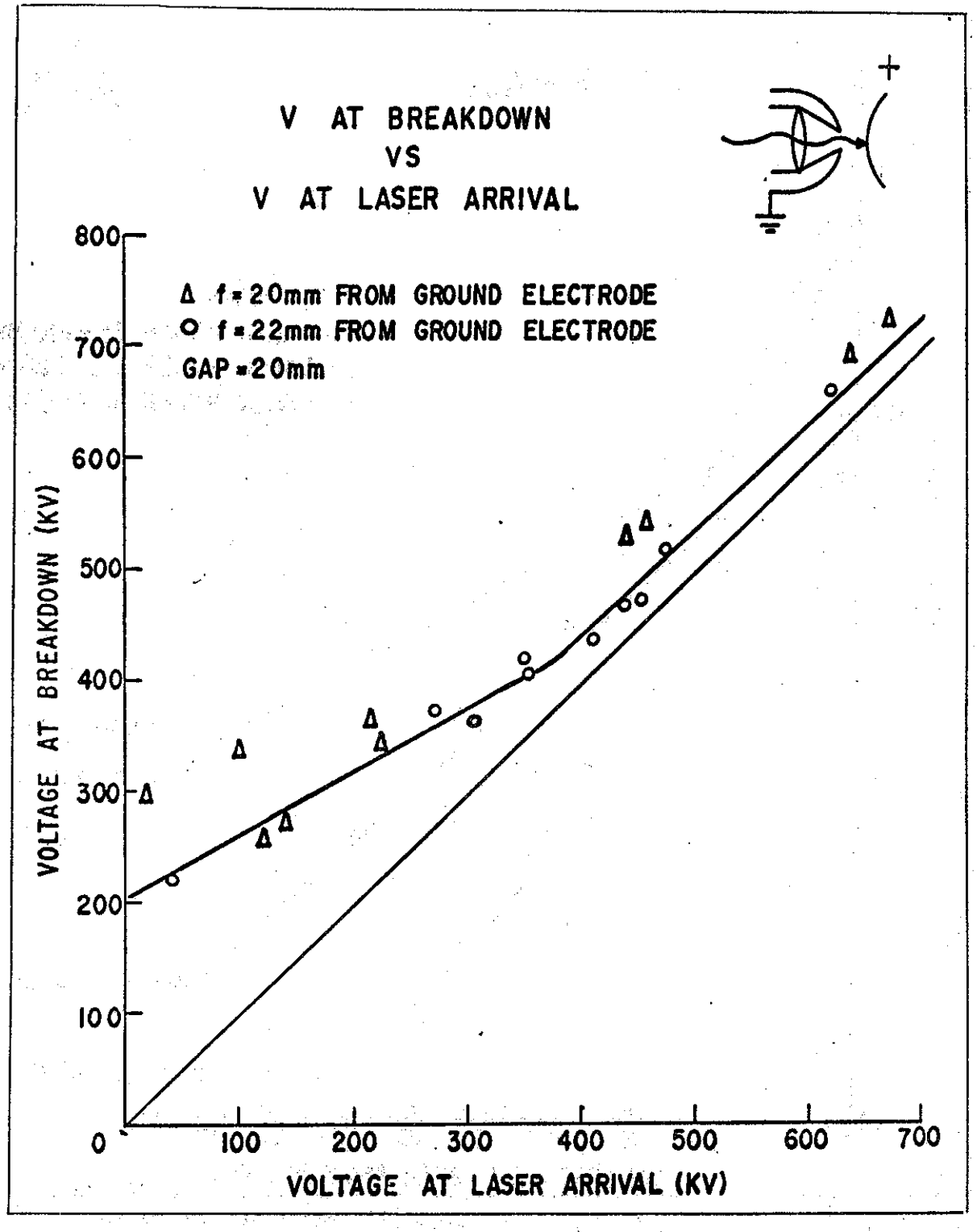

Fig. 24 Breakdown Voltage versus Voltage on Target Electrode at Laser Arrival - Positive T.E.

VI. Conclusion and Discussion

This chapter will attempt to explain some of the characteristics pointed out in the data obtained in Chapter V. The first section will correlate the proposed breakdown mechanism with the experimental data. The next section will present an estimate of the error of the parameters and an indication of the jitter. The third section discusses the main problems encountered in this experiment and recommends some solutions and future studies. The last section discusses the suitability of applying LTS technique to overvolted liquid dielectrics.

Comparison of Data with Proposed Breakdown Mechanism

The results presented in Chapter V are the first available data on a laser initiated conduction of an overvolted liquid dielectric, in particular, transformer oil. The results are consistent with the proposed streamer breakdown mechanism even though the data points are few and no more than one breakdown is represented by each point.

To corroborate the consistency of the data with the proposed streamer breakdown mechanism, a list of dependencies obtained from the proposed mechanism will be given, followed by a brief discussion of their interrelationship.

1. If streamers are the main mechanism of breakdown, the delay to breakdown of a negative target electrode should be longer than a positive target electrode, provided that the laser arrival times on the target electrode are kept constant and that the number of electrons generated by the laser is the same.

Since the laser induced electron emission seems to be independent of the target polarity (Refs. 10 and 11), a comparison of Fig. 21 with

Fig. 23 at the same focal position and comparable laser powers leads to the predicted results.

2. Since the ionization coefficient of the Townsend avalanche mechanism is proportional to the applied electric field (Ref. 18), the higher the voltage on the target electrode at laser arrival, the shorter the delay to breakdown.

Figures 21 and 23 clearly depict a variation of the delay to breakdown with the voltage on target electrode at laser arrival. Since the slope of the line is negative, this leads to the expected result that the delay to breakdown is inversely proportional to the applied electric field.

3. There should be marked increase in the delay to breakdown if the laser pulse terminates before the onset of conduction of the gap. This effect is due to the elimination of laser generation term, allowing the electron recombination term to have a more salient effect in the net rate of electron production.

In Figures 21 and 23 a marked increase in the delay breakdown at delays to breakdown in excess of 65 nsec is observed. The laser pulse used in this experiment had an average width at its base of approximately 65 nsec. The data of the positive target electrode configuration displays a hazy break in the slope due to the variation of the base pulse width from 60 to 80 nsec caused by three different oscillator rods used in the laser system.

4. The delay to breakdown should increase with decreasing laser power, provided that the laser focal position remains constant. This effect is due primarily to the initial number of electrons generated

by the first few nanoseconds of the laser pulse.

Figures 21 and 23 clearly show that for a given laser focal position, the lower power range of the laser demonstrates a higher delay to breakdown than the higher power range.

5. The delay to breakdown should exhibit a minimum at an optimum laser focal position and increase if the focal position is moved away from the optimum. This optimum focal position is basically related to the largest possible area of target illumination by the laser while still maintaining the largest number of electrons generated by the first few nanoseconds of the laser pulse, provided that the laser power is kept constant.

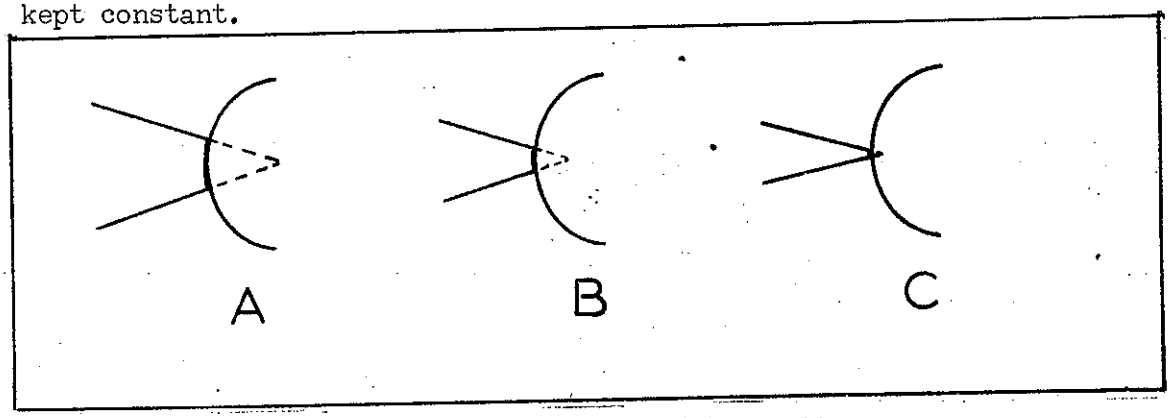

Fig. 25 Target Electrode Illumination

Figure 25 illustrates three focal positions. Position A illuminates a large area but does not contain a high power density, while position C has a high power density over a small area. Position B is the optimum compromise.

Figures 21 and 23 depict the influence of the laser focal position on the delay to breakdown. The focal position of 22 mm from the load electrode (2 mm inside the target electrode) corresponds to the focal position B of Fig. 25.

Error Estimate

The two major parameters, the laser power and the time of laser arrival on the target electrode, could not be kept at a constant value, hence no two data points were taken with the same parameters. Therefore, a thorough error analysis would be fruitless. Instead, errors associated with each individual parameter were investigated. Where errors could not be calculated, a conservative error estimate was made.

Gap width ± 0.5 mm

based on 6 measurements with the thickness gauge cross checked with a cathetometer.

Laser Focal Point ± 1.0 mm

conservative estimate, for the plasma formed by the laser could vary the focal point position by up to .5 mm at long focal lengths.

Laser Energy ± 10%

conservative estimate due to high deviation of laser pulse from Gaussian distribution due to Brillouin reflection.

Delay to Breakdown ± 0.3 nsec

determined from error associated with trace reading of 519 oscilloscope with a sweep rate of 20 nsec/cm

± 5.2 nsec

standard deviation of the two other experimental values taken at 100 nsec/cm sweep rate for 32 data points using the value of the 20 nsec/cm sweep trace as average. Applicable to delay in excess of 100 nsec.

Delay to Laser Arrival ± 5.8 nsec

error associated in reading two trace positions on 555 oscilloscope at 100 nsec/cm sweep

Breakdown Voltage	± 5%	overall error associated with 2 Mv pulser line voltage monitor and trace readings
Voltage on Target Electrode at Laser Arrival	± 5%	same breakdown voltage

Switch Jitter

The switch jitter, the difference between the maximum and minimum excursion of a particular value of the delay to breakdown, will ultimately reflect all of the above parameter's uncertainties. Since the parameters could not be held constant, an experimental determination of the switch jitter was not possible. Nevertheless, an indication of the switch jitter was obtained by doubling the difference of the delay to breakdown experimentally determined from the one calculated by the RMS approximation. Switch jitters as low as 1.2 nsec were obtained for the points near self-breakdown for a positive target electrode configuration in the laser power ranges of 150 to 220 Mw. There seems to be a trend towards higher jitter at lower laser power ranges and lower voltages on target electrode at laser arrival. Jitter will not be plotted due to the insubstantial nature of its determination.

Recommendations

The major problem encountered in this experiment was the serious degradation of the laser system due to the Brillouin reflection. The method of using a quarter wave place coupled to a Brewster tent polarizer did not effectively stop all the reflection. The higher power output needed restricts the use of many of the available optical isolators. A more thorough investigation of the dielectric reflection needs to be made before this problem can be correctly approached and

eliminated. These studies should determine the effect of the electric field, laser power, dielectric material, focusing angle, and length of propagation of the laser in the dielectric on the intensity of the Brillouin reflection.

The breakage of the last lens (in contact with the dielectric) and the optical conduit can be solved by constructing the optical system to withstand the strong shock waves generated during breakdown. The solution is basically to use a metal for the first few inches of the optical conduit that comes in contact with the dielectric and using thicker lenses properly supported along the optical axis.

The deterioration of the target electrode could be substantially reduced by using hard metal inserts, such as tungsten, in the center of the target electrode.

One other major improvement area would be to move the zero time reference point, the point where the laser system and the pulser are separated, to a point after the Marx generator, preferably to a point on the coaxial line joining the Marx generator to the target electrode. This new reference point would eliminate the 50 nsec jitter associated with the Marx generator, with respect to its trigger input, and allow a more precise selection of the time and voltage on the target electrode at laser arrival. A faster reacting Pockels cell voltage pulse generator would be needed with a maximum delay between the trigger signal and laser determined by the time that the voltage pulse takes to travel the remaining distance between the coaxial line voltage monitor and the target electrode.

Other studies with the present system would include the effect of variation of the gap spacing, voltage pulse risetime of the target

electrode, the use of different electrode materials, the use of other liquid dielectric such as water, different laser wavelengths, and different focal length optical systems on the delay to breakdown. Two other quantities of interest would be the effect of the variation of the same parameters studied for the delay to breakdown on the risetime of the output voltage pulse and the jitter associated with the delay to breakdown. Other areas of study employing minor modifications of present system would be the use of multiple channel breakdown on pulsed liquid dielectrics and a whole new field of studies involving the use of the LTS technique in overvolted gases and solid dielectrics. A provision for a gas switch has been made for the 2 Mv pulser and is currently undergoing self-breakdown tests.

Probably the most important area of future study would be a detailed study of the laser induced conduction of an overvolted dielectric. This study should be able to describe quantitatively the mechanism of the LTS breakdown and yield an analytical model for the event.

Suitability of Application of the LTS Technique to Overvolted Liquid Dielectric

This study has demonstrated that a laser initiated conduction of an overvolted transformer oil can effectively switch voltages up to 600 kv in times less than 15 nsec with jitter in the low nanosecond range.

The use of liquid dielectrics is a compromise between the feature of non-destruction of the dielectric found in gases and the very small gap spacings possible with the solid dielectrics while still retaining all the basic features of the LTS technique.

The LTS technique in pulsed liquid dielectric seems to be very dependent on laser power and the duration of the laser during conduction, hence it is advisable to use high power lasers, in levels above 300 Mw, having pulse widths comparable to or longer than the expected delay to breakdown times. Also operation in the high percent of self-breakdown voltages at laser arrival will insure low delays and jitter times.

Bibliography

1. Alston, L. L. High Voltage Technology. Oxford University Press, London (1968).

2. Barbini, S. "Coaxial Laser-Triggered Gap Study". Conference on Controlled Thermonuclear Reactions, Frascatti, Italy (1966).

3. Bettis, J. R. Private Communications.

4. Bettis, J. R., and A. H. Guenther. "Low-Jitter, High-Repetition Rate, Laser-Triggered Switching". To be published in the IEEE Journal of Quantum Electronics.

5. Clark, R. J. Laser-Triggered Switch Study. RADC Technical Report, TR-68-355. Rome Air Development Center, Griffiss AFB, New York, December 1968.

6. Cobine, J. D. Gaseous Conductors. Dover Publications, Inc., New York (1958).

7. David, C. et al. "Density and Temperature of a Laser-Induced Plasma". IEEE Journal of Quantum Electronics, QE-2:493-9 (September 1966).

8. Dawson, J. M. "On the Production of Plasma by a Giant-Pulse Laser". The Physics of Fluids, 7:981-7 (July 1964).

9. Guenther, A. H. "Recent Developments in LTS". DASIAC Special Report 80. Defense Atomic Support Agency, DASA 2155, September 1968.

10. Guenther, A. H. Private Communications.

11. Guenther, A. H. and J. R. Bettis. "Laser-Triggered Megavolt Switching". IEEE Journal of Quantum Electronics, QE-3:581-88 (November 1967).

12. Guenther, A. H. and J. R. Bettis. "Nanosecond-Synchronization, Multigap-Laser-Triggered Switching". To be published.

13. Guenther, A. H. and R. H. McKnight. "A Laser-Triggered 50 pps High Voltage Switch w/ns Jitter". Proceedings of the IEEE 55:1504 (August 1967).

14. Marolda, A. J. "Laser-Triggered Switching in a Liquid Dielectric". IEEE Journal of Quantum Electronics, 503-5 (August 1968).

15. Pendelton, W. K. and A. H. Guenther. "Investigation of a Laser-Triggered Spark Gap". Review of Scientific Instruments, 36:1546-50 (November 1965).

16. Kowel'kov, V. S. "Development of a Pulse Discharge in Liquids". Soviet Physics-Technical Physics, Vol. 6, No. 8 (February 1962).

17. Raizer, Yu P. "Breakdown and Heating of Gases under the Influence of a Laser Beam". Soviet Physics Uspekhi, 8:650-673 (March-April 1966).

18. Raether, Heinz. Electron Avalanches and Breakdown in Gases. Butterworths, Washington (1964).

19. Ready, J. F. "Mechanism of Electron Production by a Giant Pulse Laser". Phys. Rev., 37:A620-3 (January 1965).

20. Swan, D. N. "A Review of Recent Investigations into Electrical Conduction and Breakdown of Liquid Dielectrics". British J. Applied Physics, Vol. 13 (1962).

21. Strickland, D. "LTS of Solid Dielectrics", to be submitted as Thesis for M.S. Degree, W-PAFB, Ohio (AFIT).

22. Sharbaugh, A. H. and J. C. Devins. "Electrical Breakdown in Solids and Liquids". Electro-Technology, October 1961.

23. Wick, Dr. Raymond V., AFWL, Private Communications.

APPENDIX A

Optical System Focus and Spot Size Determination

The main parameters of the optical system are shown in Fig. 26. The desired result is the dependency of FFLE on H, the variable distance between lens 1 and 2. Note that the first lens is a negative focus lens while the other two are positive.

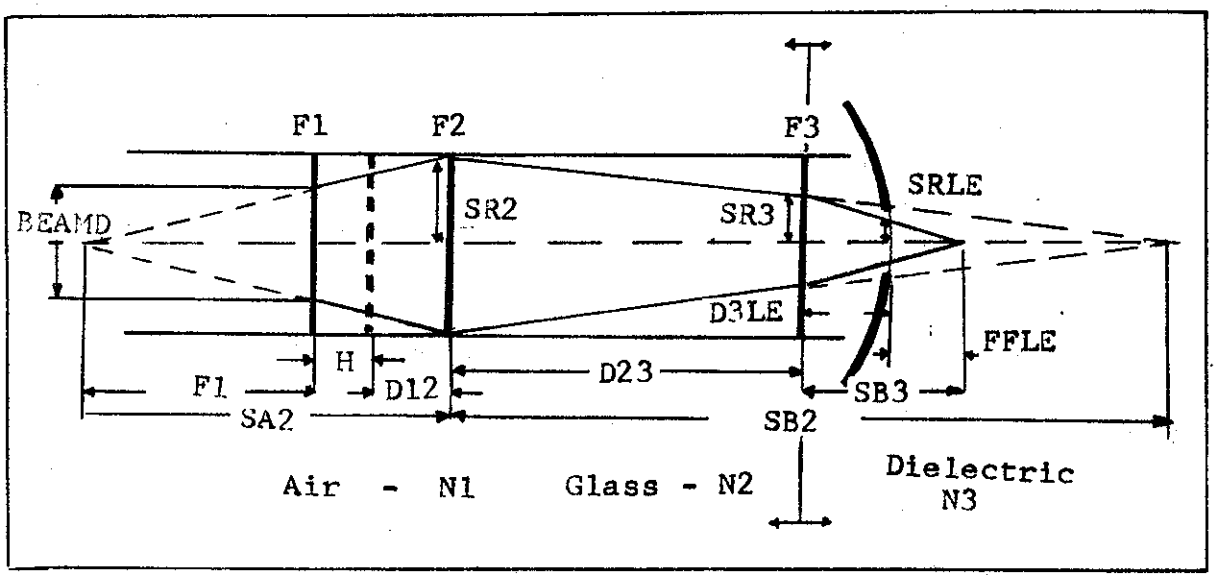

Fig. 26 Main Parameters of the Optical System and Associated Ray Diagram

Using the classical optical equation relating the focus to the object distance and image distance for a lens in air:

$$1/SA + 1/SB = 1/F \qquad (13)$$

where: SA = Image distance

SB = Object distance

F = Focal distance in air

one arrives at the image distance for the 1 and 2 lens combination for a collimated input beam:

$$SB2 = F2*SA2/(F2-SA2) \tag{14}$$

where, from Fig. 26,

$$SA2 = D12+H+F1$$

The equation relating the image and object distance for an equally radiused converging lens having a media of index of refraction N1 in the object side, N2 as the lens glass and N3 on the image side, can be derived as:

$$N1/SA + N3/SB = (2*N2 - (N1 + N3))/R \tag{15}$$

where: R = radius of lens

Solving Eq (15) for the object distance and letting:

SB = SB3

SA = SA3

N3 = index of refraction of oil

N2 = index of refraction of glass

N1 = index of refraction of air

one obtains:

$$SB3 = (N3*R*SA3)/(SA3\ (2*N2 - (N1 + N3)) - R*N1) \tag{16}$$

The dependency of the focal position of the optical system relative to the load electrode (FFLE) on the variable distance between lens 1 and 2 (H), can be obtained from Eq (16) by letting:

$$SA3 = D23 - SB2$$

where: SB2 is determined from Eq (14)

and: FFLE = SB3 - SRLE

where: SRLE = distance between load electrode and lens 3

Note that the index of refraction of the glass of the last lens is a critical value for one is subtracting two comparable values in the denominator of Eq (16). The index of refraction of the last lens can be calculated by:

$$1/F = (N-1)\ (1/R_1 + 1/R_2) \tag{17}$$

If one now allows:

$$R_1 = R_2 = R$$

$$N = N_2$$

and $$F = F_3$$

and solving for N2, one arrives at:

$$N2 = R/(2*F3) + 1 \tag{18}$$

In this experiment the parameters used were:

F1 = -5 inches

F2 = +10 inches

F3 = +2 inches

D12 = 5.6 inches

D23 = 25.0 inches

D3LE = 3.0 inches

BEAMD = 0.75 inches (beam diameter of the laser at the input of the optical conduit)

N1 = 1.00

N3 = 1.49 (determined experimentally)

R = 55.5 mm (measured experimentally)

The other parameter of interest is the spot size on the laser beam on the lens 3 and at the load electrode. The beam waist at the focus of the assembly can be calculated by using:

$$SSF = F^* \Theta \tag{19}$$

where: SSF = spot size at focus

F = equivalent focus of the system

Θ = beam divergence

The spot size on the lens 3 and the load electrode port can be calculated by similar triangles from the ray diagram of Fig. 26.

Hence:

$$BEAMD/F1 = SR2/SA2 \tag{20}$$

and:

$$SR2/SB2 = SR3/(SB2-D23) \tag{21}$$

and

$$SR3/SB3 = SRLE/FFLE \tag{22}$$

These claculations were all made with the assistance of the attached computer program. All symbols used are the same as the ones used in Fig. 26.

The calculated and experimentally determined focal positions, as a function of H, are depicted in Fig. 27.

Beam divergence was determined to be 1.6 milliradians and the spot size at the focus was determined to be 2.3 mm in diameter for a focal position of 22 mm.

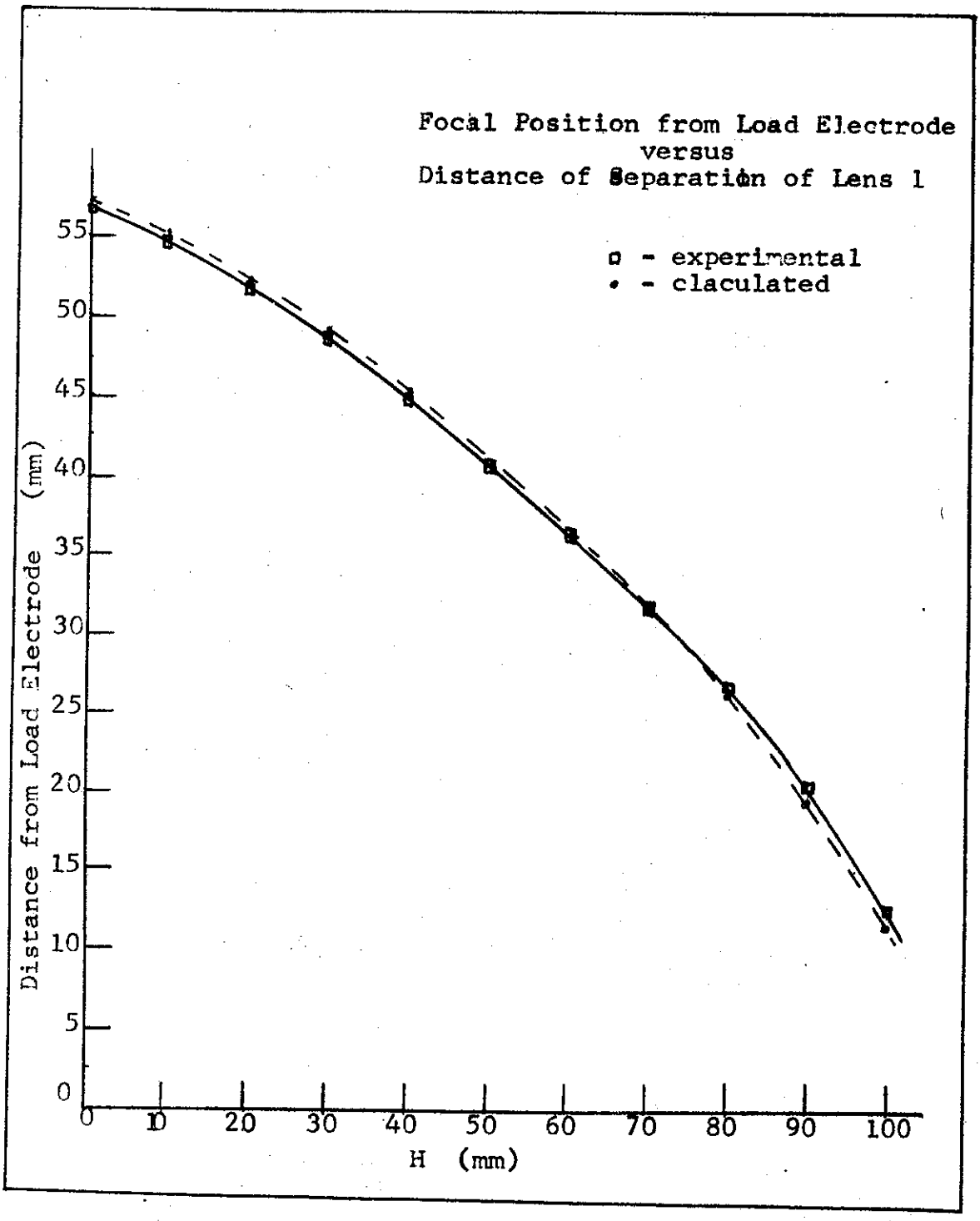

Fig. 27 Calculated and Experimental Determination of FFLE vs H

```
C  C  FOCUS AND SPOT SIZE DETERMINATION  -  LTS THESIS

C       READING LENS SYTEM PARAMETERS IN INCHES
        READ,F1,F2,F3,D12,D23,BEAMD
        READ,ON3,R3,D3LE,TEP
        PI=3.1416

C       TRANSFORMING PARAMETERS TO MM IF NEEDED
        F1M=F1*25.4*(-1.)
        F2M=F2*25.4
        F3M=F3*25.4
        D12M=D12*25.4
        D23M=D23*25.4
        BEAMR=BEAMD*25.4/2.
        D3LEM=D3LE*25.4
        TEPM=TEP*25.4

C       COMPUTING THE INDEX OF REFRACTION OF LENS 3
        GN2=R3/(2.*F3M)+1.

C       PUNCHING INPUT PARAMETERS
        PUNCH 102, F1
        PUNCH 103, F2
        PUNCH 104, F3
        PUNCH 108,GN2
        PUNCH 105, D12
        PUNCH 106, D23
        PUNCH 107, D3LE
        PUNCH 101
        PUNCH 109

C       COMPUTING THE FOCAL POINT OF THE SYSTEM AND THE SPOT
C       SIZE AND AREA
        DO 1 I=1,131,10
        H=I-1
        S2A=F1M+D12M+H
        S2B=F2M*S2A/(S2A-F2M)
        S3A=D23M-S2B
        S3B=ON3/((GN2-1.)/R3+(GN2-ON3)/R3-1./S3A)
        FFLE=S3B-D3LEM
        SR2=S2A*BEAMR/F1M
        SR3=SR2*(S2B-D23M)/S2B
        SRLE=SR3*D3LEM/S3B
        SA3=PI*SR3*SR3
        SALE=PI*SRLE*SRLE

C       PUNCHING OUT THE DESIRED RESULTS
  1     PUNCH 100,H,FFLE,SR3,SRLE,SA3,SALE

C       FORMATS
 100    FORMAT(/,3X,F5.1,5(3X,F7.2))
```

```
101  FORMAT(//,5X,1HH,7X,4HFFLE,7X,3HSF3,6X,4HSRLE,7X,
    1 3HSA3,6X,4HSALE)
102  FORMAT(4X,4HF1 =, F5.1,1X,6HINCHES)
103  FORMAT(/,4X,4HF2 =  F5.1,1X,6HINCHES)
104  FORMAT(/,4X,4HF3 =, F5.1,1X,6HINCHES)
105  FORMAT(/,3X,5HD12 =, F5.1,1X,6HINCHES)
106  FORMAT(/,3X,5HD23 =, F5.1,1X,6HINCHES)
107  FORMAT(/,2X,6HD3LE =,,F5.1,1X,6HINCHES)
108  FORMAT(/,3X,5HGN3 =,F6.3)
109  FORMAT(5X,14HDIMENSION = MM)
     STOP
     END
```

APPENDIX B

10 OHM Coaxial Line Voltage Pulse Analysis

The equivalent series circuit of the pulse charge system used in this experiment can be represented as shown in Fig. 28.

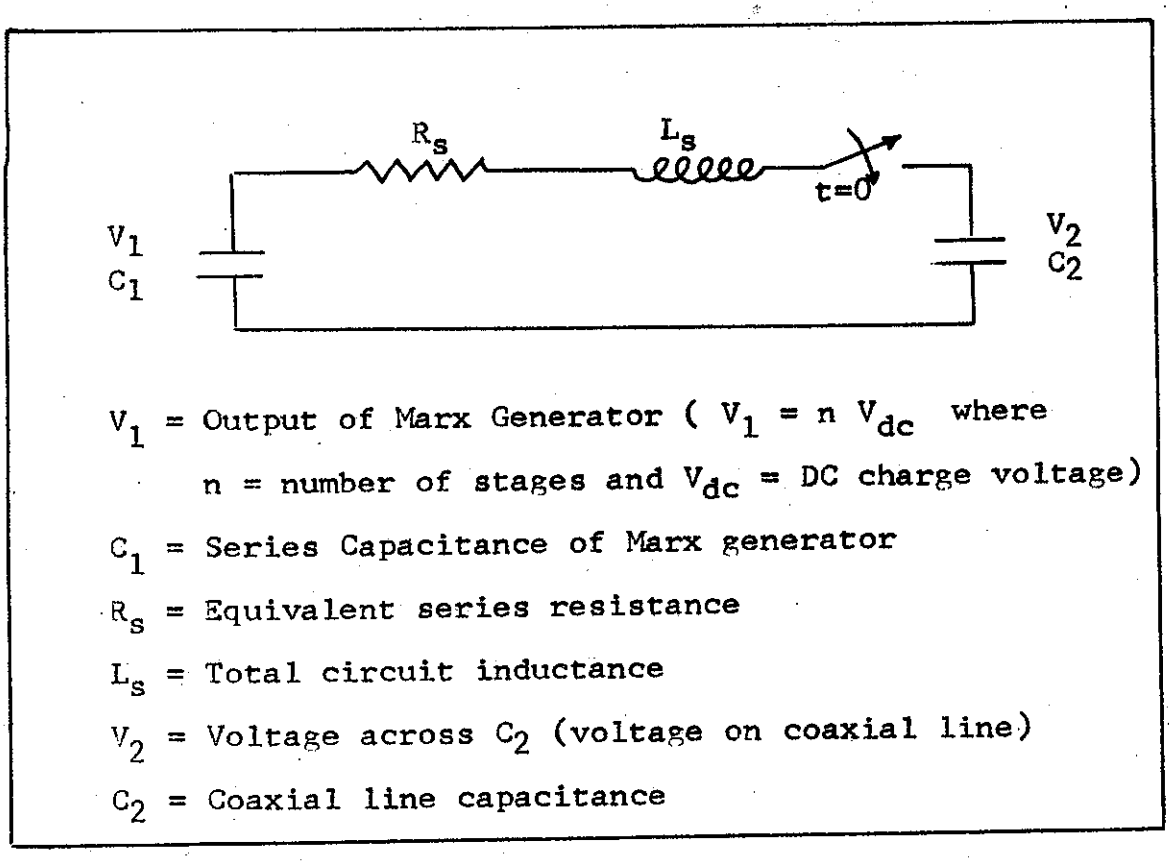

V_1 = Output of Marx Generator ($V_1 = n\ V_{dc}$ where n = number of stages and V_{dc} = DC charge voltage)

C_1 = Series Capacitance of Marx generator

R_s = Equivalent series resistance

L_s = Total circuit inductance

V_2 = Voltage across C_2 (voltage on coaxial line)

C_2 = Coaxial line capacitance

Fig. 28 Equivalent Circuit of Pulse Charge System

An analysis of the above circuit yields for V_2:

$$V_2(t) = \frac{C_1 V}{C_1 + C_2}\left[1 - e^{-\alpha t}\frac{(\alpha^2+\beta^2)^{1/2}}{\beta}\sin(\beta t + \phi)\right] \qquad (23)$$

where:

$$\alpha = \frac{R_s}{2L_s}$$

$$\beta = \sqrt{\frac{C_1+C_2}{L_s C_1 C_2} - \left(\frac{R_s}{2L_s}\right)^2}$$

$$\phi = \tan^{-1}\frac{\beta}{\alpha}$$

If $\left(\frac{R_s}{2L_s}\right)^2$ is small compared to $\frac{C_1+C_2}{L_s C_1 C_2}$, as in a Marx Generator, Eq 23 can be approximated to:

$$V_2 \cong \frac{C_1 V_1}{C_1+C_2}\left[1 - e^{-\alpha t}\cos(\omega t)\right]$$

If the circuit resistance is low and if C_1 is much greater than C_2, the voltage on C_2 can approach two times the initial voltage on C_1 at the end of the first half-cycle.

The risetime of the voltage pulse on the coaxial line can be varied by changing the choke that connects the Marx Generator with the coaxial line, hence changing the circuit's inductance.

No analytical calculations were made for the voltage pulse. Figures 29 and 30 depict the experimentally determined pulse waveform taken from the voltage monitor of the 10 ohm coaxial line. The negative pulse is plotted with a vertical negative axis to facilitate a comparison between both polarities. These plots represent an average of 5 shots per polarity. The self-breakdown voltage for the positive pulse was found to be (700 ±35) kv while the negative pulse exhibited a (600 ±35) kv self-breakdown.

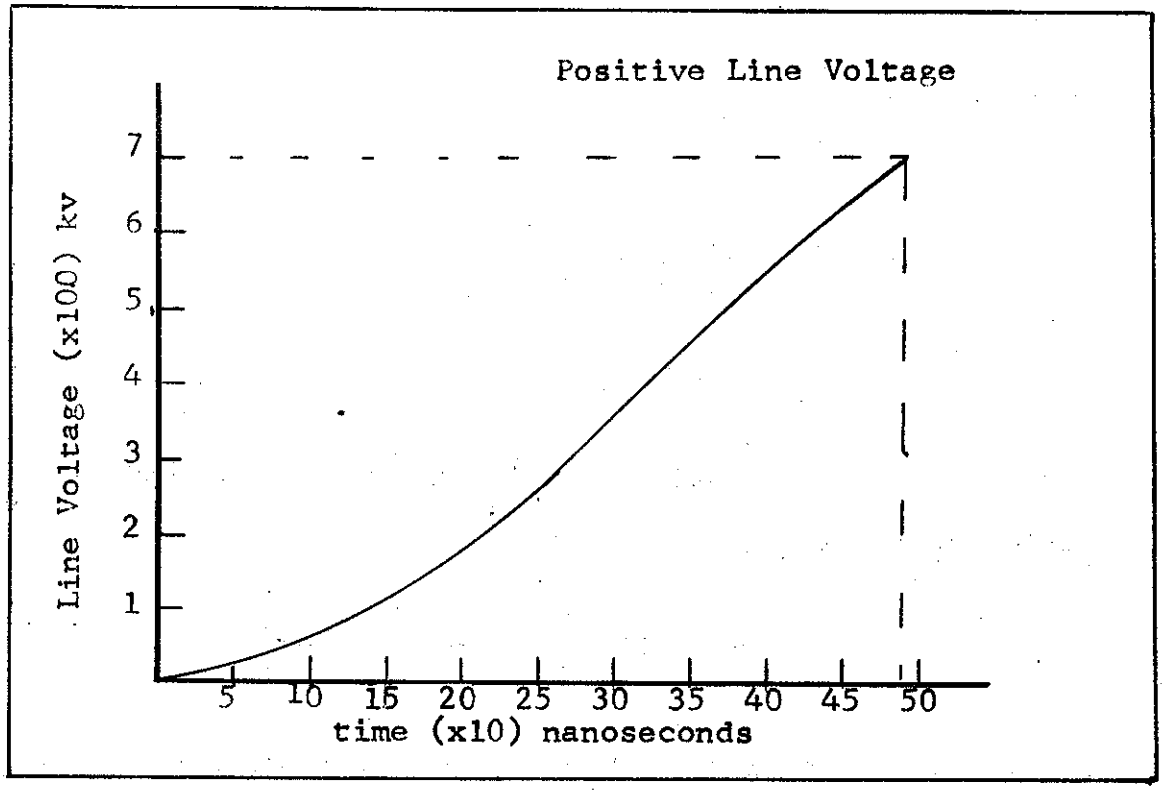

Fig. 29 Positive Line Voltage

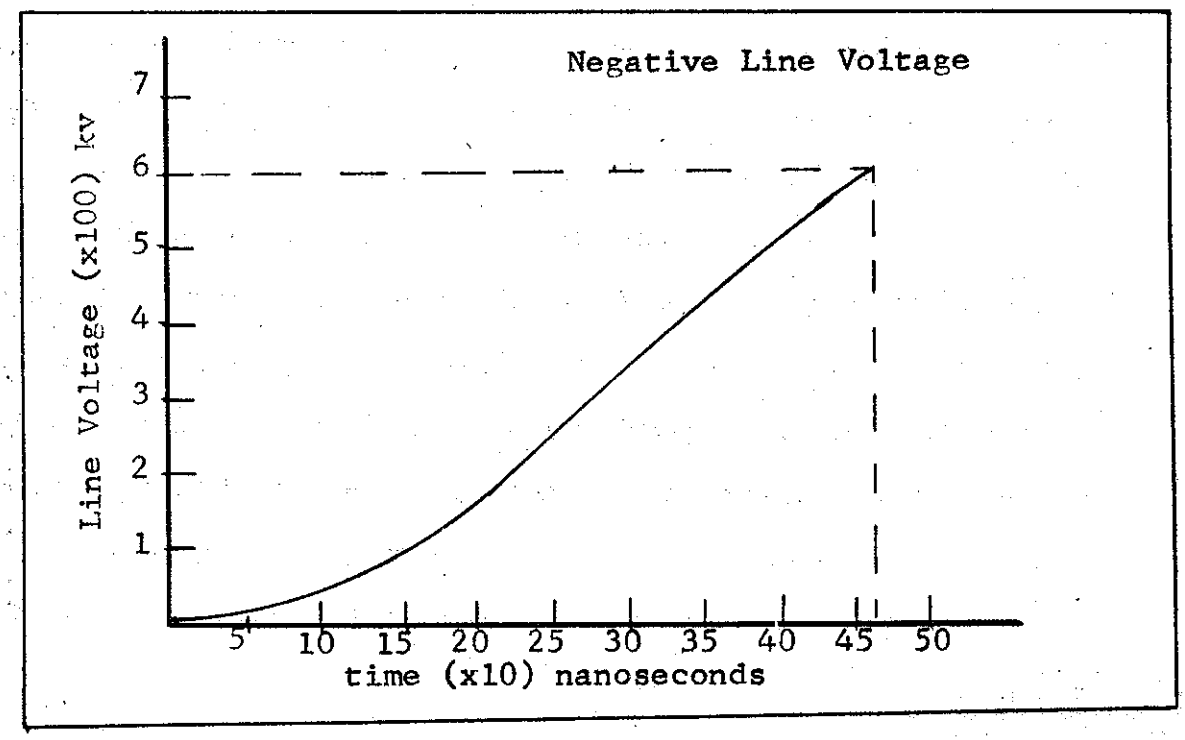

Fig. 30 Negative Line Voltage

APPENDIX C

Root Mean Square Program

The RMS program used in this experiment is a highly modified AFIT AID program. It is capable of storing all the data points desired for a specific run and the operator can select the different x or y he desires by inserting the called for indicators via a typewriter input. The program will perform the RMS best fit to the given data points in log-log, semi-log or numerical form. The output features the RMS deviation for each point and converts the calculated values back to numericals if needed. The standard deviation of the points is also output together with the equation describing the best fit.

The program is self-explanatory and each step can be easily traced, hence no detailed analysis will be given. One should remember that this program was designed so that the user has immediate feedback via a typewriter output, and can be easily converted to non-operator assisted once the desired runs are determined.

```
      JOB  LEAST SQUARES FITTING FOR LTS THESIS
*     ORIGIN 15000

C     RESERVING STORAGE SPACE
      DIMENSION X(30),Y(30),YY(30),DELTY(30),A(10,11)
      DIMENSION HH(30),SS(30),LZ(30)
      DIMENSION AA(30),BB(30),CC(30),DD(30),EE(30)
      DIMENSION FF(30),GG(30)

C     DETERMINING IF NEW DATA OR NEW X IS TO BE USED
 1020 TYPE 1008
      ACCEPT,L
      IF(L) 1021,1022,1023

C     READING IN DATA
 1022 READ,MMM
      DO 1030 I=1,MMM
      READ 1017,AA(I),BB(I),CC(I),DD(I),EE(I),FF(I)
     1 GG(I),HH(I),SS(I)
      TYPE 1013,AA(I)
 1030 CONTINUE

C     ACCEPTING FOCUS POSITON AND TARGET ELECTRODE POLARITY
      TYPE 1014
      ACCEPT,PTE
      TYPE 1007
      ACCEPT,FFF

C     SELECTING X
 1023 TYPE 1009
      TYPE 1010
      ACCEPT,N
      IF(N) 2000,3000,4000
 2000 DO 5000 I=1,MMM
      LZ(I)=AA(I)
      Y(I)=HH(I)
      X(I)=EE(I)
 5000 CONTINUE
      KK=MMM
      IF(PTE) 5010,5011,5011
 5010 PUNCH 1015
      GO TO 5012
 5011 PUNCH 1016
 5012 CONTINUE
      PUNCH 1116
      PUNCH 1006,FFF
      PUNCH 1002
      PUNCH 1112
      PUNCH 1005
      GO TO 8000
 3000 J=1
```

```
      DO 6000 I=1,MMM
      IF(FF(I)) 2010,2020,2010
2020  GO TO 6000
2010  X(J)=FF(I)
      LZ(J)=AA(I)
      Y(J)=HH(I)
      J=J+1
6000  CONTINUE
      KK=J-1
      IF(PTE) 5013,5014,5014
5013  PUNCH 1015
      GO TO 5015
5014  PUNCH 1016
5015  CONTINUE
      PUNCH 1116
      PUNCH 1006,FFF
      PUNCH 1003
       PUNCH 1112
      PUNCH 1005
      GO TO 8000
4000  J=1
      DO 7000 I=1,MMM
      IF(GG(I)) 3100,3200,3100
3200  GO TO 7000
3100  X(J)=GG(I)
      Y(J)=HH(I)
      LZ(J)=AA(I)
      J=J+1
7000  CONTINUE
      KK=J-1
      IF(PTE) 5016,5017,5017
5016  PUNCH 1015
      GO TO 5018
5017  PUNCH 1016
5018  CONTINUE

C     PUNCHING OUT TABLE HEADINGS
      PUNCH 1116
      PUNCH 1006,FFF
      PUNCH 1004
      PUNCH 1112
      PUNCH 1005
8000  PUNCH 1011

C    PUNHING OUT DATA POINTS USED
      PUNCH 1001,(LZ(J),J=1,KK)

C     SPECIFYING ORDER OF POLINOMIAL AND RESIDUE TOLERANCE
      KN=0
       CON=1.
      NN=1
      LI=0
      TOL=1.
```

```
C       CHECKING THAT ENOUGH DATA IS GIVEN FOR REQUESTED
C       POLYNOMIAL
        IF(KK-1-NN)95,96,96
 95     PUNCH 107,NN
        STOP

C       DETERMINING WHETHER DATA IS TO BE FITTED TO NUMERICAL,
C       SEMI-LOG, OR LOG-LOG CURVE AND PERFORMING LOG
C       OPERATIONS
        IF(LI)155,152,150
 150    DO 151 I=1,KK
 151    X(I)=CON*LOG(X(I))
 152    DO 154 I=1,KK
 154    Y(I)=CON*LOG(Y(I))

C       CONSTRUCTING NORMAL EQUATIONS AND PUTTING COEFFICIENTS
C       INTO MATRIX
 155    N=NN+1
        M=N+1
        DO 102 I=1,N
        LL=I-1
        A(I,M)=0.
        DO 102 J=1,N
        A(I,J)=0.
        K=J+I-2
        DO 102 II=1,KK
        IF(J-1)101,100,101
 100    WHY=Y(II)*X(II)**LL
        A(I,M)=A(I,M)+WHY
 101    TEMP=X(II)**K
 102    A(I,J)=A(I,J)+TEMP

C       SOLVING THE SIMULTANEOUS EQUATIONS BY THE JORDAN
C       METHOD

C       SEARCHING FOR LARGEST PIVOT ELEMENT
        DO 8 K=1,N
        MM=K+1
        TEMP=A(K,K)
        I=0
        IF(K-N)41,45,41
 41     DO 42 II=MM,N
        IF(ABS(TEMP)-ABS(A(II,K)))46,42,42
 46     TEMP=A(II,K)
        I=II
 42     CONTINUE

C       CHECKING FOR SINGULARITY AND NEED FOR ROW INTERCHANGE
 45     IF(TEMP)47,14,47
 47     IF(I)43,49,43
```

```
C       INTERCHANGING ROWS
 43     DO 44 J=1,M
        TEMP=A(I,J)
        A(I,J)=A(K,J)
 44     A(K,J)=TEMP

C       DIVIDING ROW BY PIVOT ELEMENT
        TEMP=A(K,K)
 49     DO 5 J=MM,M
 5      A(K,J)=A(K,J)/TEMP

C       SUBTRACTING MULTIPLES OF PIVOT ROW FROM OTHER ROWS
        DO 8 I=1,N
        IF(I-K)6,8,6
 6      TEMP=A(I,K)
        DO 7 J=1,M
 7      A(I,J)=A(I,J)-TEMP*A(K,J)

C       COMPUTING AND STORING RESIDUES AND TOTAL RMS ERROR
        SMDY2=0.
        DO 121 J=1,KK
        WHY=A(1,M)
        DO 120 I=1,NN
        TEMP=A(I+1,M)*X(J)**I
 120    WHY=WHY+TEMP
        YY(J)=WHY
        DELTY(J)=Y(J)-WHY
        TEMP=DELTY(J)*DELTY(J)
 121    SMDY2=SMDY2+TEMP
        Q=KK
        TEMP=SQRT(SMDY2/Q)

C        COMPUTING THE STANDARD DEVIATION
         TEMP2=SQRT(SMDY2/(Q-2.))
         SIGY=TEMP2

C        COMPUTING THE STANDARD DEVIATION OF THE SLOPE
 600     XKK=KK
         XSUM=0.0
         XXSUM=0.0
         DO 650 I=1,KK
         XXSUM=XXSUM+X(I)*X(I)
         XSUM=XSUM+X(I)
 650     CONTINUE
         D=XKK*XXSUM
         SIGS=SIGY*SQRT(XKK/(D-(XSUM*XSUM)))

C       COMPARING TOTAL RMS ERROR WITH SPECIFIED TOLERANCE
        IF(KN)198,201,198
 198    IF(NN-10)203,201,201
 203    IF(TEMP-TOL)201,201,204
 204    IF(NN-KK+1)205,201,201
```

```
C       RETURNING TO BEGINNING FOR FIT TO HIGHER ORDER,
C       IF NECESSARY
 205    NN=NN+1
        GO TO 155

C       PUNCHING TABLE HEADINGS
 201    PUNCH 530
        PUNCH 125
        PUNCH 126
C       OUTPUTTING RESIDUES AND TOTAL RMS ERROR
        DO 202 J=1,KK
 202    PUNCH 127,LZ(J),X(J),Y(J),YY(J),DELTY(J)
        PUNCH 128, TEMP
         PUNCH 528,SIGY
        PUNCH105,NN,KK

C       CHECKING FOR NUMERICAL, SEMI-LOG, OR LOG-LOG
C       OUTPUT EQUATION
        J=0
        IF(LI)160,161,162
 160    PUNCH 175
        PUNCH 106, A(1,M), J, (A(I+1,M),I,I=1,NN)
         GO TO 800
 161    PUNCH 175
        PUNCH 166, A(1,M), J, (A(I+1,M),I,I=1,NN)
         PUNCH 529,SIGS
        CCT=A(1,M)
        EET=A(2,M)
        CCT=EXP(CCT)
        PUNCH 8050
        PUNCH 8010, CCT,EET,SIGS
         GO TO 800
 162    PUNCH 174
        PUNCH 166, A(1,M), J, (A(I+1,M),I,I=1,NN)
 800     CONTINUE

C        CONVERSION BACK TO NON-LOG
        IF(LI) 701,500,501
 501    DO 601 I=1,KK
 601    X(I)=EXP(X(I))
 500    DO 602 I=1,KK
        Y(I)=EXP(Y(I))
 602    YY(I)=EXP(YY(I))
        SMDY2=0.0
        DO 603  I=1,KK
        DELTY(I)=Y(I)-YY(I)
        TEMP=DELTY(I)*DELTY(I)
 603    SMDY2=SMDY2+TEMP
        Q=KK
        TEMP=SQRT(SMDY2/Q)
```

```
C       COMPUTING THE STANDARD DEVIATION
        TEMP2=SQRT(SMDY2/(Q-2.))
        SIGY=TEMP2

C       PUNCHING TABLE HEADINGS
        PUNCH 700
        PUNCH 125
        PUNCH 126

C       OUTPUTTING CONVERTED RESIDUES AND TOTAL RMS ERROR
        DO 620 J=1,KK
 620    PUNCH 127, LZ(J),X(J),Y(J),YY(J),DELTY(J)
        PUNCH 128, TEMP
        PUNCH 528,SIGY
        GO TO 701


C      FORMAT STATEMENTS
 105   FORMAT(/20HBEST POLYN OF DEGREE,I2,5H FOR ,I2,
     1 12H DATA PTS IS,/,1X)
 106   FORMAT(12X,3HY =,5X,1PE16.7,I13,/(20X,1PE16.7,I13))
 107   FORMAT(46HNOT ENOUGH DATA PTS FOR A POLYNOMIAL
     1 OF DEGREE,I2)
 125   FORMAT(//,3X,4HSHOT,2(8X,5HGIVEN),6X,8HCOMPUTED,6X,
     1 9HDELTA Y =)
 126   FORMAT(2X,6HNUMBER,9X,1HX,12X,1HY,12X,1HY,10X,
     1 9HY(G)-Y(C),/)
 127   FORMAT(3X,I4,3(6X,F7.2),6X,F9.4)
 128   FORMAT(/17X,31HTOTAL ROOT MEAN SQUARE RESIDUE=,
     1 1PE16.7)
 166   FORMAT(8X,7HLOG Y =,5X,1PE16.7,I13,/(20X,1PE16.7,I13))
 174   FORMAT(23X,11HCOEFFICIENT,7X,14HPOWER OF LOG X,/1X)
 175   FORMAT(23X,11HCOEFFICIENT,9X,10HPOWER OF X,/1X)
 528   FORMAT(/,17X,32HSTANDARD DEVIATION OF Y VALUES =,
     1 1PE16.7)
 529   FORMAT(/ /,17X,29HSTANDARD DEVIATION OF SLOPE =,
     1 1PE16.7)
 530   FORMAT(///,17X,15HSEMI-LOG VALUES)
 700    FORMAT(////,17X, 27HCONVERSION TO ORIGINAL DATA)
  14    PUNCH 110
 110   FORMAT(15HMATRIX SINGULAR)
1001   FORMAT(I7,I7,I7)
1002   FORMAT(6HX=NSEC)
1003   FORMAT(5HX=VLA)
1004   FORMAT(6HX=PSBD)
1005   FORMAT(/)
1006   FORMAT(/,6HFOCUS=,F7.2,23H MM FROM LOAD ELECTRODE)
1007   FORMAT(6HFOCUS=)
```

380 (91)

```
1008  FORMAT(28HO=NEW DATA, -1=STOP, 1=NEW X)
1009 FORMAT(8HSELECT X)
1010 FORMAT(22H-1=NSEC, 0=VLA, 1=PSBD)
1011 FORMAT(13HDATA PTS USED,/)
1112 FORMAT(5HY=DTB)
1013 FORMAT(F7.1)
1014 FORMAT(13H+TE=1, -TE=-1)
1015 FORMAT(25HTARGET ELECTRODE NEGATIVE)
1016 FORMAT(25HTARGET ELECTRODE POSITIVE)
1116 FORMAT(13HGAP= 20.00 MM)
1017 FORMAT(F5.1,F6.2,F7.2,F8.2,F8.2,F8.2,F7.2,F8.2,
    1 F8.2,F7.2)
1018 FORMAT(//////)
8010 FORMAT(/,8X,3HY =,1PE11.3,6H EXP((,1PE11.3,3H +-,
    1 1PE11.3,5H ) X))
8011 FORMAT(77X,2H..)
8050 FORMAT(//,20HEXPONENTIAL EQUATION)
701  CONTINUE
     PUNCH 1018
     PUNCH 8011
     GO TO 1020
1021 STOP
     END
*    EOJ
```